

RESEARCH

Open Access



# Conformational antigenic heterogeneity as a cause of the persistent fraction in HIV-1 neutralization

Philippe Colin<sup>1,3</sup>, Rajesh P. Ringe<sup>1,4</sup>, Anila Yasmeen<sup>1</sup>, Gabriel Ozorowski<sup>2</sup>, Thomas J. Ketas<sup>1</sup>, Wen-Hsin Lee<sup>2</sup>, Andrew B. Ward<sup>2</sup>, John P. Moore<sup>1</sup> and P. J. Klasse<sup>1\*</sup>

## Abstract

**Background** Neutralizing antibodies (NAbs) protect against HIV-1 acquisition in animal models and show promise in treatment of infection. They act by binding to the viral envelope glycoprotein (Env), thereby blocking its receptor interactions and fusogenic function. The potency of neutralization is largely determined by affinity. Less well explained is the persistent fraction, the plateau of remaining infectivity at the highest antibody concentrations.

**Results** We observed different persistent fractions for neutralization of pseudovirus derived from two Tier-2 isolates of HIV-1, BG505 (Clade A) and B41 (Clade B): it was pronounced for B41 but not BG505 neutralization by NAb PGT151, directed to the interface between the outer and transmembrane subunits of Env, and negligible for either virus by NAb PGT145 to an apical epitope. Autologous neutralization by poly- and monoclonal NAbs from rabbits immunized with soluble native-like B41 trimer also left substantial persistent fractions. These NAbs largely target a cluster of epitopes lining a hole in the dense glycan shield of Env around residue 289. We partially depleted B41-virion populations by incubating them with PGT145- or PGT151-conjugated beads. Each depletion reduced the sensitivity to the depleting NAb and enhanced it to the other. Autologous neutralization by the rabbit NAbs was decreased for PGT145-depleted and enhanced for PGT151-depleted B41 pseudovirus. Those changes in sensitivity encompassed both potency and the persistent fraction. We then compared soluble native-like BG505 and B41 Env trimers affinity-purified by each of three NAbs: 2G12, PGT145, or PGT151. Surface plasmon resonance showed differences among the fractions in antigenicity, including kinetics and stoichiometry, congruently with the differential neutralization. The large persistent fraction after PGT151 neutralization of B41 was attributable to low stoichiometry, which we explained structurally by clashes that the conformational plasticity of B41 Env causes.

**Conclusion** Distinct antigenic forms even of clonal HIV-1 Env, detectable among soluble native-like trimer molecules, are distributed over virions and may profoundly mold neutralization of certain isolates by certain NAbs. Affinity purifications with some antibodies may yield immunogens that preferentially expose epitopes for broadly active NAbs, shielding less cross-reactive ones. NAbs reactive with multiple conformers will together reduce the persistent fraction after passive and active immunization.

**Keywords** HIV-1 neutralization, Broadly active neutralizing antibodies (bNAbs), Persistent fraction, Efficacy, Antigenic heterogeneity, Stoichiometry, Binding kinetics

\*Correspondence:

P. J. Klasse

pek2003@med.cornell.edu

Full list of author information is available at the end of the article



© The Author(s) 2023. **Open Access** This article is licensed under a Creative Commons Attribution 4.0 International License, which permits use, sharing, adaptation, distribution and reproduction in any medium or format, as long as you give appropriate credit to the original author(s) and the source, provide a link to the Creative Commons licence, and indicate if changes were made. The images or other third party material in this article are included in the article's Creative Commons licence, unless indicated otherwise in a credit line to the material. If material is not included in the article's Creative Commons licence and your intended use is not permitted by statutory regulation or exceeds the permitted use, you will need to obtain permission directly from the copyright holder. To view a copy of this licence, visit <http://creativecommons.org/licenses/by/4.0/>. The Creative Commons Public Domain Dedication waiver (<http://creativecommons.org/publicdomain/zero/1.0/>) applies to the data made available in this article, unless otherwise stated in a credit line to the data.

## Background

Neutralizing antibodies (NAbs), whether induced by infection or vaccination, are the best correlate of protection against viral infections in general [1–3]. Neutralization is defined as interrupting the viral replicative cycle before the first virally encoded transcriptional event by the binding of the neutralizing agent to the virion surface [4]. The mechanism of neutralization of enveloped viruses, as far as is known, is always a direct or indirect block of any step in the entry process, such as receptor interaction and fusion of the envelope with a cellular membrane [4]. To mediate that block, a certain occupancy of NAbs on the virions is necessary and sufficient [4, 5].

The elicitation of broadly active NAbs (bNAbs), capable of neutralizing most circulating variants of HIV-1, remains a central albeit elusive goal of vaccine development [6–13]. The difficulties arise from a number of defenses against neutralizing responses that the HIV-1 envelope glycoprotein (Env), the sole target for NAbs, has developed: extreme sequence variability in surface-exposed regions of the protein, poor reactivity with germline B-cell receptors, conformational and oligomeric masking of functionally important sites, and a malleable glycan shield [10, 11, 14, 15]. Holes in the glycan shield on the Env immunogen due to absence of glycosylation sites or the underoccupancy on actual sites tend to be targeted by narrow autologous responses [16–22].

Soluble Env trimers of the SOSIP.664 design derived from the BG505 (Clade A) and B41 (Clade B) HIV-1 isolates have been shown by crystallography and cryo-electron microscopy (EM) at high resolution to adopt near-native structures and in binding analyses to expose bNAb epitopes preferentially [23–31]. We used both of these trimers to investigate binding parameters that might explain differences in neutralization plateaus for the corresponding two viruses [32, 33].

Studies of NAbs uniformly measure their potency, i.e. the concentration or dilution that gives a certain reduction of the viral infectivity. More neglected is the efficacy of neutralization, *i.e.*, the maximum inhibition achieved at the highest NAb concentrations, or its converse, dubbed the persistent fraction (PF) [4, 34–37]. This plateau of the neutralization curve is sometimes obvious and well below 100%; in other cases log–log plots of relative infectivity as a function of NAb concentration can reveal substantial PFs that remain hidden in traditional plots with % neutralization on the y axis [4].

We analyzed the neutralization potency and efficacy of three bNAbs, 2G12 (outer-domain oligomannose epitope [38]), PGT145 (trimer-specific apical epitope [39, 40]), and PGT151 (gp120-gp41-interface epitope [41, 42]) against two Env-pseudotyped viruses (PVs): BG505 [25,

43] and B41 [26]. We compared these quantitative neutralization properties with the kinetics, affinities, and stoichiometries of binding to SOSIP trimers derived from the same isolates. And we detected antigenic heterogeneity by affinity fractionation of both PV virions and SOSIP trimers, thereby explaining contributions to the PF that apply even to clonal, *i.e.* genetically homogeneous virus (*cf.* [44]).

Progress towards eliciting bNAbs by active vaccination was recently made through such strategies as germline targeting, immunogen presentation on virus-like particles, sequential immunization, and mRNA delivery [16, 17, 20, 45]. Once bNAbs can be induced, their efficacy can arguably be as important as their potency in preventing transmission [4, 46]. Furthermore, bNAb therapy is showing great promise [9, 14, 15, 47, 48]. In line with our findings, combinations of bNAbs in passive immunization and aiming for multiple specificities in active immunization are rational strategies for counteracting antigenic heterogeneity and thereby reducing the PF, which could otherwise undermine therapeutic and preventive success [4, 5, 7, 49].

## Results

### Outline of rationale and experimental steps in hypothesis testing

We chose the B41 isolate for further study because of its large PFs in neutralization by autologous SOSIP-trimer-induced NAbs; BG505 is neutralized by corresponding NAbs to near completion and was therefore selected as a suitable comparator [32, 33]. Further reasons for choosing these two viruses were that we have made stable, soluble trimers derived from the *env* genes, and high-resolution structural and spectroscopic conformational data for these trimers are available to help interpret our new data [23–30, 39, 50]. Additionally, we have experience in purifying these two trimers with the bNAbs 2G12, PGT145, and PGT151 [18, 23–26, 31, 51].

On the hypothesis that the cause of the PF we are trying to identify in autologous neutralization also affects neutralization by bNAbs, we first analyzed the potency and efficacy of the three bNAbs used for affinity purification. PGT151 uniquely left a substantial PF with B41 (references to Figures are given in the detailed descriptions of the findings below). To exclude excess viral antigen as a cause of PFs, we also titrated the virus and found a constant proportion of infectivity over a wide range of variation in viral dose.

We then sought to test the hypothesis of heterogeneous antigenicity in Env as the cause of the PF. We devised a method for depleting virion populations of the subset of particles with the strongest antigenicity for an antibody.

We built a molecular three-dimensional model of the B41 trimer, based on a previously published structure [52] to illustrate the discrete epitopes for 2G12, PGT145, and PGT151. As done for 2G12- and PGT145-affinity purification [18, 23–26, 31, 51], we showed by negative-stain electron microscopy (NS-EM) that PGT151-affinity purification also yields monodisperse, ~100% native-like B41 trimer. We next purified the trimer preparations with 2G12, PGT145, or PGT151, depleted the 2G12-purified trimer population using PGT145 or PGT151, and used SPR and ELISA to analyze how various bNABs bound to the different fractions. Detailed kinetic and stoichiometric SPR analyses of PGT145- and PGT151-Fab binding to BG505 and B41 trimer populations revealed a reduced stoichiometry of PGT151 binding to the B41 trimer, in agreement with the larger PF with that bNAB. Finally, we sought a structural explanation for the differences in stoichiometry by modeling PGT151 binding to the B41 trimer, based on known structures and the tendency of that trimer to adopt a partially open conformation [26, 27].

In what follows, we describe the investigational steps outlined above in more detail but in the same sequence.

### Comparative neutralization potency and efficacy

A comparison of neutralization by the three bNABs 2G12, PGT145, and PGT151 showed differential potencies and efficacies against BG505 and B41 PV. All three bNABs left negligible PFs of BG505 PV. Similar efficacies notwithstanding, the potencies differed ( $IC_{50}$  was 0.91  $\mu\text{g/ml}$  for 2G12, 0.20  $\mu\text{g/ml}$  for PGT145, and 0.043  $\mu\text{g/ml}$  for PGT151). The potency ranking from highest to lowest for BG505 was thus: PGT151, PGT145, and 2G12 (Fig. 1A). In contrast, although B41 PV was neutralized to close to 100% by 2G12 and PGT145, PGT151 left a PF of 21%. The potencies differed also against B41 ( $IC_{50}$  was 7.0  $\mu\text{g/ml}$  for 2G12, 0.14  $\mu\text{g/ml}$  for PGT145, and 0.39  $\mu\text{g/ml}$  for PGT151), thus ranking downwards in a different order: PGT145, PGT151, and 2G12 (Fig. 1B).

An excess of the viral antigen that is the target of NABs would be a potential cause of incomplete neutralization. Through specific adsorption, the concentration of free NAB would then decline significantly so that it approaches or falls below the dissociation constant,  $K_D$ . Then the ensuing occupancies would not be predicted by the ratio of the added NAB concentration over the  $K_D$ . If the virus inoculum is sufficiently small, however, the decline in concentration of free NAB is negligible

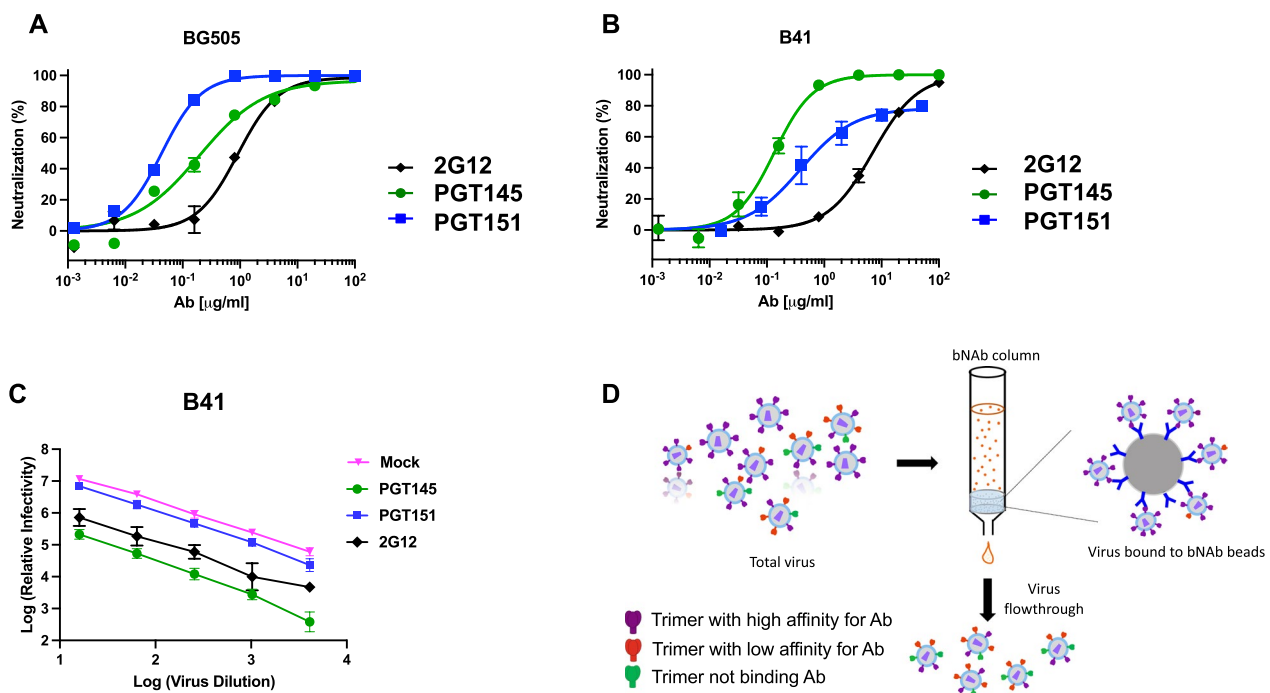


**Fig. 1** Neutralization efficacy of BG505 and B41 pseudovirus. The extent of neutralization (%) of PV in a TZM-bl assay is plotted as a function of NAB concentration ( $\mu\text{g/ml}$ ); means  $\pm$  s.e.m. of 2–4 replicate titrations are shown. Neutralization by the three bNABs 2G12 (N332 glycan), PGT145 (V2-apex), and PGT151 (gp41-gp120 interface) of BG505 PV (**A**) and B41 (**B**) gave different potencies and efficacies. **C** The  $\log_{10}$  of the relative remaining infectivity after neutralization by bNAB at a fixed concentration (50  $\mu\text{g/ml}$ ) is plotted as a function of the  $\log_{10}$  of varied viral inoculum dilution. **D** The schematic shows the procedure for partial depletion of a PV preparation by the absorption of virions binding most avidly to bNABs on beads

and the proportion of virus that is neutralized remains approximately constant over a range of inoculum doses. Figure 1C shows the titration of virus against a high, constant concentration of bNAb (50  $\mu\text{g/ml}$ ). The drop in  $\log_{10}$  infectivity signal was approximately constant for the three bNAb over a 2.5- $\log_{10}$  range of viral input. Insufficient bNAb amount relative to virus is thus ruled out as a contributor to the PF under the experimental conditions: the relative neutralization adhered to the percentage law of neutralization [53]. The neutralization with varied bNAb concentration and varied viral input together also illustrate the partial independence of potency and efficacy: PGT151 was more potent than 2G12 before reaching the PF, but 2G12 was the more effective of the two (Fig. 1B and C).

### Antigenic heterogeneity of Env spikes on PV

To dissect antigenic heterogeneity in the PV population, we conjugated bNAb to Sepharose beads to deplete inocula of virions most reactive with the respective bNAb (Fig. 1D). The depletion is designed to be partial. The number and density of Env spikes with at least some antigenicity will determine the avidity of virion capture (Fig. 1D). Meaningful depletions were possible only for B41 PV. Depletion of BG505 PV left negligible and insufficient infectivity for a mechanistic dissection.

Henceforth, we focus on B41 neutralization potency and efficacy, in particular seeking explanations in antigenic heterogeneity of its large PF with PGT151. Depletion of the B41 PV by PGT145- and PGT151-conjugated beads gave differentially neutralized fractions (Fig. 2). Neutralization by PGT145 was consistently but only moderately more potent for PGT151- than PGT145-depleted PV, mock-depleted PV falling in between; the neutralization efficacies were close to 100% after the three depletions (Fig. 2). Neither neutralization by 2G12 nor VRC01, directed to a CD4-binding-site (CD4bs) epitope, was affected by the depletions. In contrast, PGT151 neutralization was 2 orders of magnitude more potent against PGT145- than PGT151-depleted PV, the potency for mock-depleted PV falling between, somewhat closer to the former than the latter. The corresponding PF was reduced for PGT145- compared with mock-depleted PV, whereas the PGT151 neutralization of PGT151-depleted PV was so diminished that no PF plateau could accurately be extrapolated. ASC202, directed to an interface epitope overlapping that for PGT151, neutralized with potencies ranking as for PGT151 against the three depleted PV fractions but with smaller shifts and without yielding detectable PFs for any depletion. Finally, N123-VRC34.01 (hereafter VRC34.01), also specific for an interface epitope [54], weakly and partially neutralized the PGT145-depleted PV (40% at 50  $\mu\text{g/ml}$ ) but had no

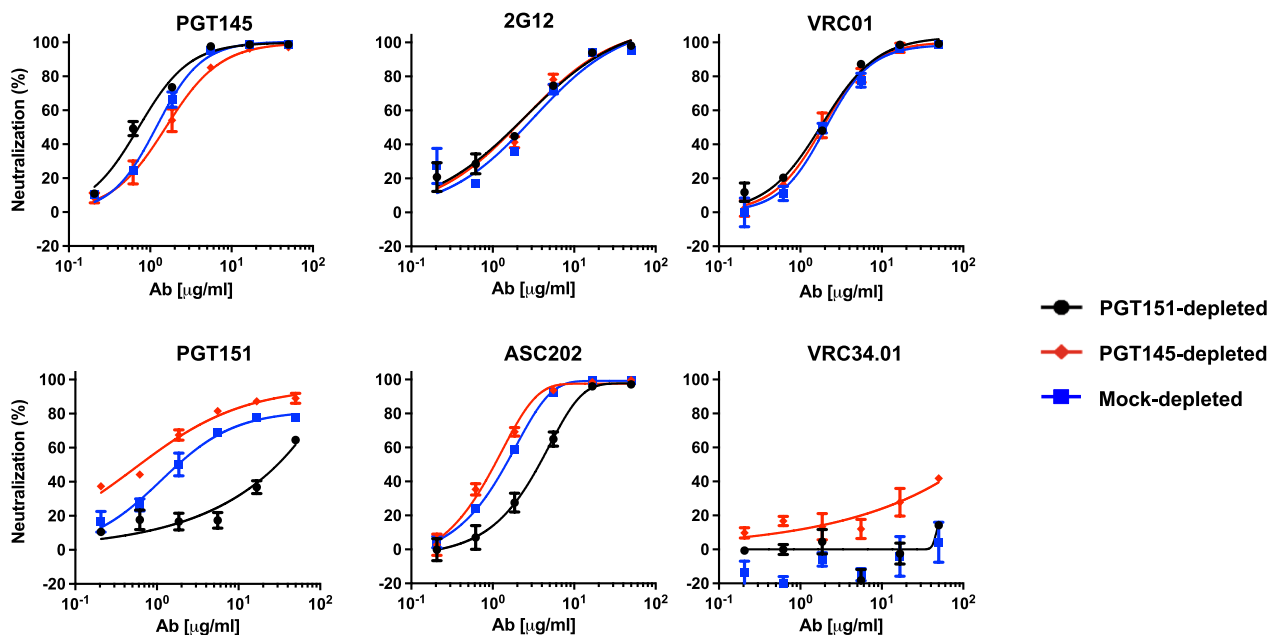


**Fig. 2** Neutralization of bNAb-depleted B41 PV by bNAb. The extent of neutralization (%) is plotted as a function of bNAb concentration ( $\mu\text{g/ml}$ ). PV was first incubated with Sepharose beads covalently conjugated with bNAb PGT145 or PGT151 or mock-conjugated (see color-coded legend). The unbound virions were then tested for neutralization by the NAb indicated in each diagram in a TZM-bl neutralization assay. The extent of neutralization (%) is plotted as a function of bNAb concentration ( $\mu\text{g/ml}$ ), so that potencies rise as curves are shifted from right to left

effect against the other two fractions. We elaborate on explanations for sufficient stability of the antigenic differences to allow the observed depletions in the Discussion, building on the relevant following findings.

Eight sera from B41 SOSIP.664-immunized rabbits [18, 32] yielded a range of PFs against mock-depleted PV: 5–60% (Fig. 3). Neutralization potency and efficacy were consistently lower against the PGT145-depleted than the PGT151-depleted PV, the curves for the mock-depleted PV falling in between. Just as the sizes of the PFs varied greatly among the sera, however, so did the differences in PFs with each serum for the three depletions.

Two monoclonal NABs (mNABs), 13A and 16D, were isolated from two of these B41-immunized rabbits (5713

and 5716 [32, 33]). Like the sera, they neutralize the autologous Tier-2 PV well, and a mutant with a knock-in N289-glycan is markedly less well neutralized [33, 55]. Congruently with the results for the sera, neutralization potency and efficacy were lower against the PGT145-depleted than the PGT151-depleted PV, whereas curves for the mock-depleted PV fell in between; the corresponding PF differences were clear with both mNABs (Fig. 4). Although it is not feasible to elute infectious PV from the bNABs on the beads, the depletion results suggest that the more PGT151-reactive Env on the PV virions, which preferentially tethers them to the beads, exposes this off-target glycan-hole epitope less well than does the more PGT145-reactive Env.

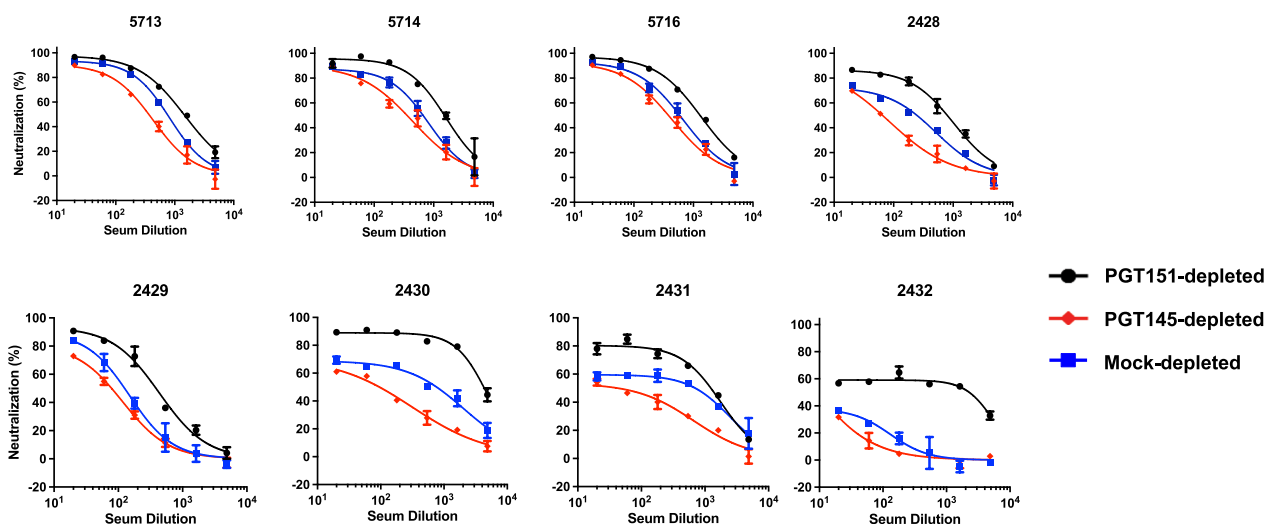


**Fig. 3** Neutralization of bNAB-depleted B41 PV by sera from immunized rabbits. The extent of neutralization (%) of PV depleted as in Figs. 1D and 2 is plotted as a function of Ab serum dilution factor. Thus, in contrast to diagrams for monoclonal Abs, the potency rises as curves are shifted from left to right

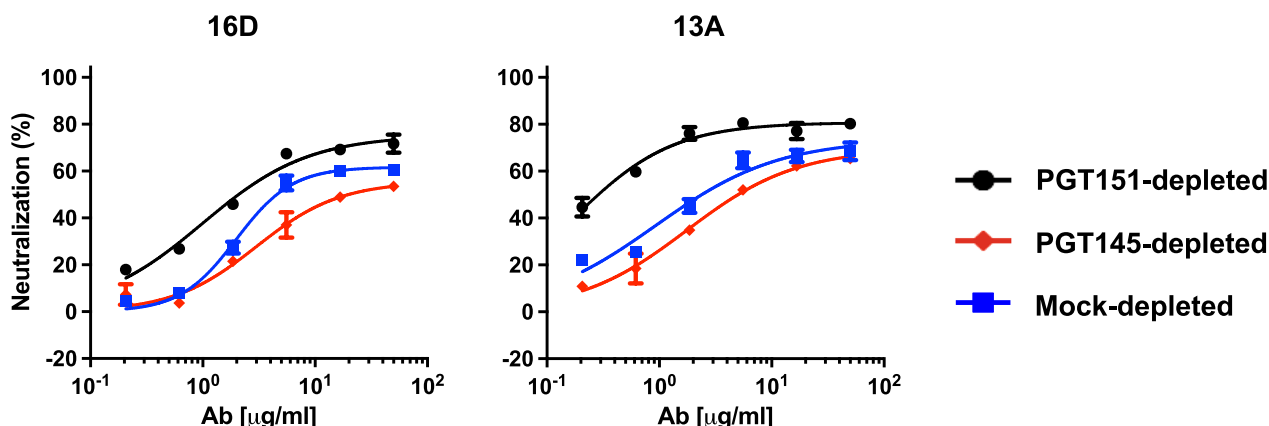


**Fig. 4** Neutralization of bNAB-depleted B41 PV by mNABs from immunized rabbits. The extent of neutralization (%) of PV depleted as in Figs. 1D, 2, and 3 is plotted as a function of autologous mNAB concentration (µg/ml). In contrast to the plots for the sera in Fig. 3, the potency rises as curves are shifted from right to left

### Differential purification and antigenicity of soluble native-like Env SOSIP.664 trimers

The 2G12, PGT145, and PGT151 epitopes, as well as the N289 residue, which is part of a glycan-hole epitope on wild-type B41 Env, are shown in their oligomeric-structural contexts in Fig. 5A. The model is based on the crystal structure of the B41 SOSIP.664 trimer, with the addition of Man<sub>9</sub> oligomannose glycans to all potential N-linked glycosylation sites (PNGS) [52, 55]. Figure 5A

illustrates how the glycan-knock-in mutation at N289 fills a defect in the glycan shield, thereby blocking a prominent epitope for autologous NAbs [32]. That soluble trimers with structures similar to the native one shown in Fig. 5A can be obtained by 2G12- and PGT145-affinity purification has been shown multiple times for BG505 and B41 SOSIP.664 trimers by NS-EM [18, 23–26, 31, 51]. As found here, the PGT151-purified B41 SOSIP.664 trimer also appeared trimeric by BN-PAGE (Fig. 5B).

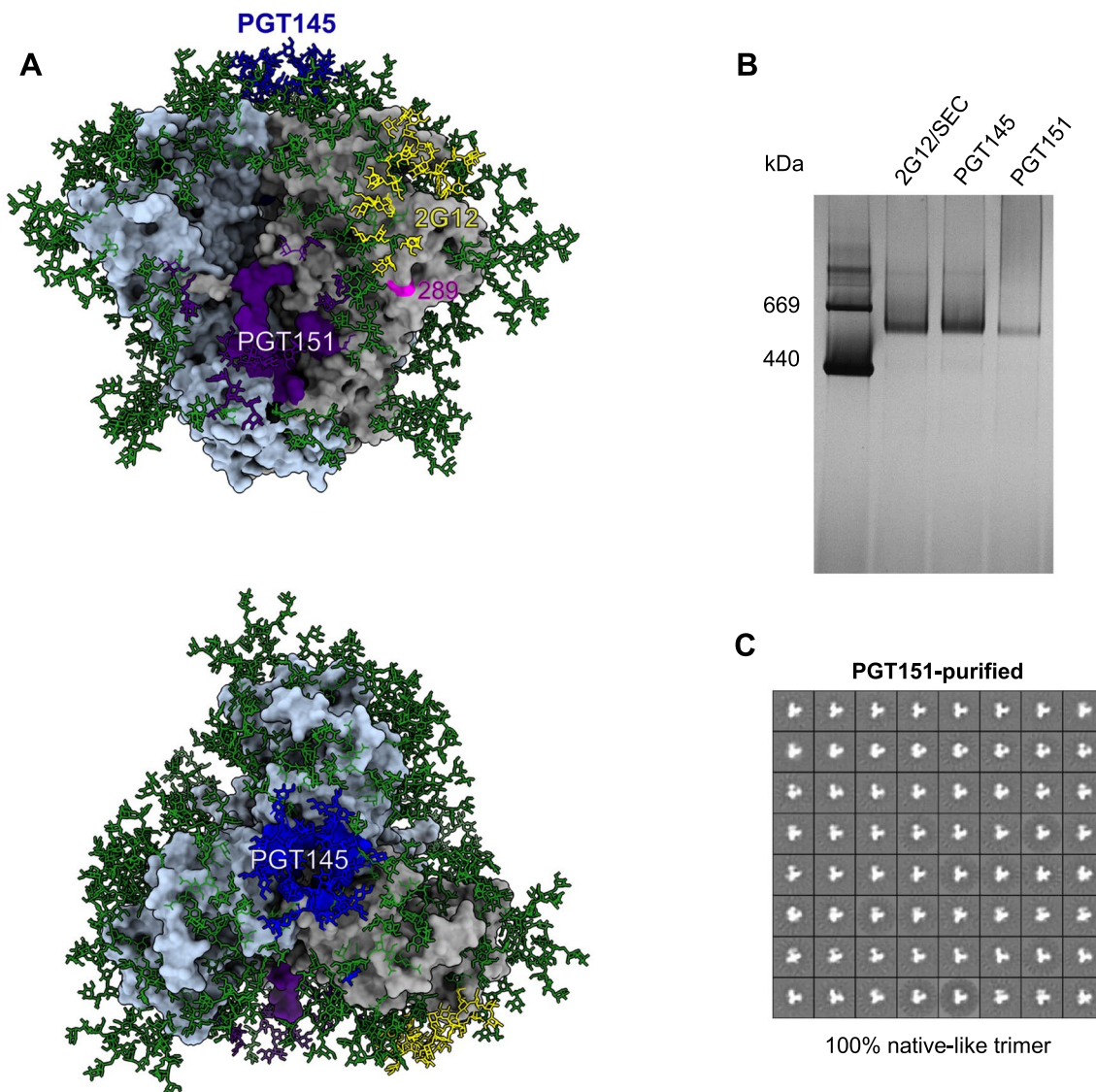


**Fig. 5** B41 SOSIP.664 trimer. **A** A surface-rendered model of the B41 SOSIP.664 trimer (PDB 6MCO [52]) oriented with the apex up (top model) or viewed from above (bottom model). The peptidic surface is gray on one protomer and light blue on the other two. Man<sub>9</sub> glycans were added to the published model [52] and are depicted as sticks and colored green unless they are directly involved in the epitopes of the three bNABs used for affinity purification, in which case they are colored as the rest of the epitope. Contacts with PGT145 are colored blue, with 2G12 yellow, and with PGT151 purple. N289, which is not part of a PNGS in B41 SOSIP.664, is colored magenta. **B** Purified Env proteins were analyzed by electrophoresis in 4–12% Bis-Tris BN-PAGE gels with Coomassie-blue staining. 2 μg protein per well was loaded from each purification. **C** NS-EM analyses of unliganded the B41 SOSIP.664 trimer purified by PGT151-affinity chromatography. The propeller-like, triangular particles show 100% native-like trimer molecules

NS-EM 2D-class averages revealed intact trimer molecules with overall movement of the 3 protomeric lobes relative to the center, suggesting substantial conformational diversity within the basic native structure, as is typical for B41 trimers (Fig. 5C) [26]. Particles lacking a central triangular mass, a defect that characterizes non-native structures, such as those of uncleaved Env [56], were not observed. We have thus demonstrated that PGT151-affinity purification also yields native-like B41 SOSIP.664 trimer molecules, which enabled us to perform bNAb-binding analyses with differentially purified native-like trimers and explore the antigenic heterogeneity further.

In pursuit of explanations of the large PF specifically with PGT151 against B41 PV, we first used ELISA to explore the binding of bNAbs to B41 SOSIP.664 trimer purified by 2G12-, PGT145-, or PGT151-affinity chromatography and thereafter by SEC (Additional file 1: Fig. S1). 2G12 bound similarly to the three trimer preparations. PGT145 bound strongly to PGT145- and 2G12-purified trimers but considerably less well to PGT151-purified trimer. Conversely, PGT151 bound strongly only to the trimer purified with PGT151 itself

and weakly to 2G12- and PGT145-purified trimer. The differential binding of VRC34.01, which like PGT151 is directed to an interface epitope [54], was similar to that of PGT151. The two autologous rabbit mNAbs resembled each other in binding profile: strong binding to PGT145- and 2G12-purified, and substantially weaker to PGT151-purified trimer. These results suggest that PGT151 has a high affinity for a subpopulation of the antigenically heterogeneous trimer molecules, which exposes the 289-glycan-hole epitope less well than the most PGT145-reactive subpopulation.

The bNAb binding to differentially purified B41 and BG505 SOSIP.664 trimers was then compared by SPR (Fig. 6). Binding to the BG505 SOSIP.664 trimer was indistinguishable after 2G12, PGT145, and PGT151 purification by the bNAbs VRC01, VRC34.01, 35O22 (gp120-gp41 interface [57]), and 3BC315 (gp41, inter-protomeric [58]), as well as by the two purification bNAbs, PGT145 and PGT151, whereas 2G12 and PGT121 binding subtly favored the 2G12-purified form.

In contrast, the B41 SOSIP.664 trimer showed a wide range of distinct antigenicities resulting from the different purifications (Fig. 6A). VRC01 bound marginally

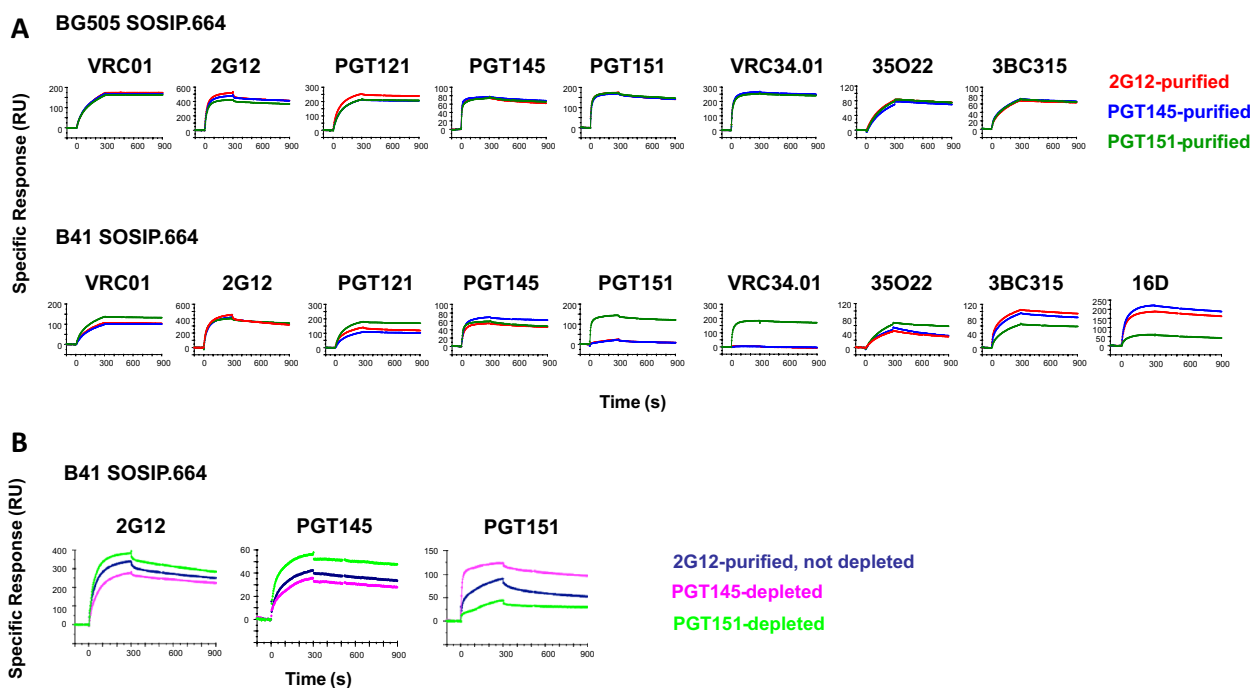


**Fig. 6** SPR analysis of bNAb binding to bNAb-purified and -depleted BG505 and B41 SOSIP.664. Sensorgrams for individual bNAbs are shown. **A** BG505 (top) and B41 (bottom) SOSIP.664 trimers were affinity-purified the bNAbs 2G12, PGT151, or PGT145 in a first step and thereafter by SEC. To the right in the B41 row is the sensorgram for the autologously neutralizing rabbit mNAb 16D. Each sensorgram shows the response after background subtraction on the y axis (response units, RU) over time after start of injection on the axis (s). Association was monitored for 300 s and dissociation for 600 s. **B** B41 SOSIP trimer was first 2G12-affinity and then SEC-purified and thereafter depleted by passage through Sepharose columns with the bNAbs PGT151 or PGT145 or no antibody on the beads. The flowthrough trimer was immobilized and analyzed by SPR as in **A**. The sensorgrams represent 2–3 highly similar replicates

better to the PGT151-purified trimer than to the other two; 2G12 did not differentiate clearly among the three purifications. Although the PGT121 epitope includes the N332 glycan, which is central to the 2G12 epitope, PGT121 bound most strongly to PGT151-purified, and least strongly to PGT145-purified, trimer; binding to 2G12-purified trimer was intermediate. PGT145 binding to the trimer purified with itself was somewhat stronger than to the other two forms. The greatest differences occurred with PGT151 and VRC34.01 binding, the binding to the PGT151-purified trimer strongly dominating, whereas binding to neither of the other two forms was detectable with VRC34.01. Another interface bNAb, 35O22, bound better to the PGT151-purified trimer than to the other two, although the difference was smaller than for PGT151 itself and VRC34.01. 3BC315, binding interprotomerically and closer to the base than the interface bNAbs, gave another distinct ranking, PGT151-purified binding being markedly lower. Finally, the autologous mNAb 16D bound well to PGT145- and 2G12-purified trimer and only to a low level to the PGT151-purified trimer, indicating, again, that the most PGT151-reactive trimer molecules in the trimer population expose the 289-glycan-hole epitope less well or present it in a shape that fits the paratope less well than does the PGT145-purified trimer. The exposure of the 289-centered epitope may require a flexibility that the most PGT151-reactive forms lack [41].

The affinity-purified fractions of trimer correspond to the *eluate* in the chromatography. Because of the distinct antigenic effects of the differential affinity-purification specifically on the B41 SOSIP.664 trimer, we also *depleted* it with bNAb-affinity columns, collecting the *effluent*. Thus, 2G12 and SEC purification of the B41 SOSIP.664 trimer followed by PGT145, PGT151, or mock depletion gave further evidence of antigenic heterogeneity. Depletion with PGT145 reduced PGT145 binding to the trimer and depletion with PGT151 increased it (the same ranking over a narrower span occurred with 2G12 binding). Conversely and more markedly, depletion with PGT151 reduced PGT151 binding to the trimer and depletion with PGT145 increased it (Fig. 6B).

The sensorgrams for Fab titrations against BG505 and B41 SOSIP.664 trimers are shown in Fig. 7. Kinetic constants  $k_{on}$  and  $k_{off}$ , the dissociation constant,  $K_D$ , and the stoichiometry,  $S_m$ , were first obtained by Langmuir modeling (Table 1). Langmuir modeling gave passable fits,  $\chi^2$  ranging from 0.13 to 0.65; the values of the kinetic constants were significant:  $T$  values [= mean/(s.e.m.)] were > 10, except for  $k_{off}$  of the highly stable PGT145-Fab binding to PGT145-purified B41 SOSIP.664, which fell below the level of detectability,

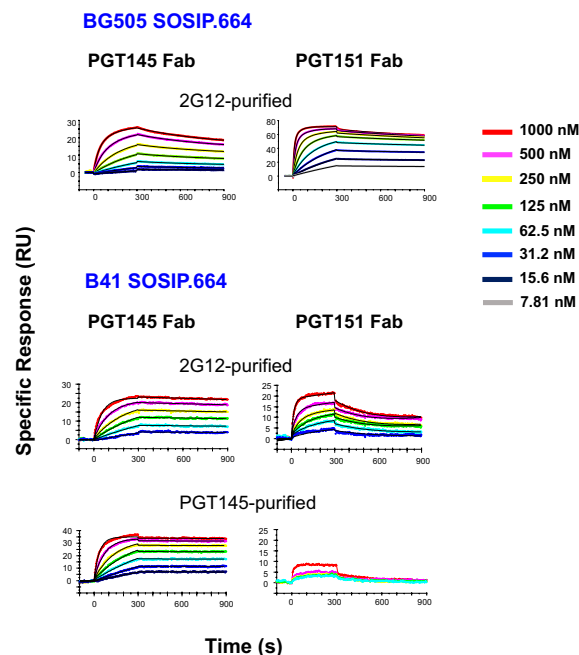


**Fig. 7** bNAb-Fab binding to BG505 and B41 SOSIP.664 SOSIP.664. Fabs of PGT145 or PGT151 were injected over trimer immobilized freshly in each cycle at concentrations as indicated in the color-coded legend. BG505 SOSIP.664 trimer was 2G12-purified and B41 SOSIP.664 trimer 2G12- or PGT145-purified, as indicated. Each sensorgram shows the response after background subtraction on the y axis (response units, RU) over time after start of injection on the axis (s). Association was monitored for 300 s and dissociation for 600 s. The model-fitted functions (heterogeneous-ligand for BG505 and Langmuir for B41) are shown as thin black curves. The sensorgram for PGT151 Fab binding to PGT145-purified B41 trimer has no model curves because no model fitted to the weak binding. The number of replicate titrations is given in Table 1

$10^{-5}$  ( $s^{-1}$ ). For the other combinations the  $T$  values were in the range 51–545 (Additional file 1: Table S1).

The  $k_{on}$  value for PGT151 binding to BG505 SOSIP.664 was higher and the  $k_{off}$  value lower than for PGT145 binding: the net effect was a 14-fold higher intrinsic affinity of PGT151 than PGT145 Fab (Table 1), in agreement with the higher neutralization potency of PGT151; the partial bivalency of IgG binding to virions is not expected to change  $IC_{50}$  ratios but to enhance potency weakly or moderately [4, 31, 59, 60].

The kinetic analysis of binding to B41 SOSIP.664 showed that the PGT145 purification gave a somewhat higher (60%)  $k_{on}$ , a lower  $k_{off}$ , falling below detectability, and lower  $K_D$ , whose upper limit only therefore could be determined, than the corresponding values for 2G12-purified trimer (Table 1). Those differences suggest an antigenic heterogeneity in the B41 SOSIP.664 population, which is marked after 2G12 purification and diminished by PGT145 purification.

**Table 1** Langmuir modeling<sup>a</sup>

SOSIP.664 trimer	Fab	Affinity purification	$k_{on}^b$ (1/Ms)	$k_{off}^b$ (1/s)	$K_D^b$ (nM)	$S_m^b$
BG505	PGT145	2G12 (n=3)	$1.8 \times 10^4 \pm 3.7 \times 10^2$	$5.1 \times 10^{-4} \pm 2.0 \times 10^{-6}$	$29 \pm 0.69$	$0.74 \pm 6.8 \times 10^{-3}$
	PGT151	2G12 (n=2)	$8.7 \times 10^4 \pm 3.5 \times 10^2$	$1.8 \times 10^{-4} \pm 5.0 \times 10^{-7}$	$2.0 \pm 1.3 \times 10^{-2}$	$1.9 \pm 7.5 \times 10^{-3}$
B41	PGT145	2G12 (n=3)	$2.0 \times 10^4 \pm 8.8 \times 10^2$	$1.2 \times 10^{-4} \pm 1.5 \times 10^{-5}$	$6.2 \pm 0.28$	$0.63 \pm 1.6 \times 10^{-2}$
		PGT145 (n=3)	$3.2 \times 10^4 \pm 2.3 \times 10^3$	$< 10^{-5}$	$< 0.5$	$0.87 \pm 4.8 \times 10^{-2}$
	PGT151	2G12 (n=3)	$4.0 \times 10^4 \pm 4.1 \times 10^3$	$3.1 \times 10^{-3} \pm 2.4 \times 10^{-4}$	$77 \pm 5.0$	$0.45 \pm 1.5 \times 10^{-2}$
		PGT145 (n=2)	Minimal binding: < 10 RU			

<sup>a</sup> Tabulated values are means  $\pm$  S.E.M of *n* independent replicates

<sup>b</sup>  $k_{on}$  and  $k_{off}$  are the on- and off- rate constants, respectively;  $K_D$  is equilibrium dissociation constant =  $k_{off}/k_{on}$ .  $S_m$  denotes the stoichiometry, i.e., number of Fab molecules per trimer

The most central explanatory findings were the differences in stoichiometry between PGT145 and PGT151 binding to BG505 and B41 SOSIP.664 trimers. The stoichiometric  $S_m$  value of PGT145 Fab binding to BG505 trimer, 0.74, approached the ideal maximum of 1.0 for this epitope [31, 39, 61]; that of PGT151 Fab binding to BG505 trimer was close to its previously described maximum of 2.0 [31, 41, 62]. PGT145 bound with distinct stoichiometries to 2G12-purified and PGT145-purified B41 trimer,  $S_m = 0.63$  and  $0.87$ , respectively, showing that the 2G12-purified trimer population contains species lacking detectable affinity for this antibody. Most striking was the low PGT151 stoichiometry for 2G12-purified B41 trimer: 4.2-fold lower than for BG505. PGT151 Fab bound so poorly to PGT145-purified B41 trimer that the data could not be modeled (Table 1). Taken together, these findings strongly suggest subpopulations among the B41 SOSIP.664-trimer molecules with distinct antigenicities. The heterogeneity manifesting itself as reduced  $S_m$  values comprises binding and non-binding forms.

We investigated potential heterogeneities within the binding populations further by applying a heterogeneous-ligand model. Four criteria can be applied to evaluate the meaningfulness of the more complex model: first, a marked reduction in  $\chi^2$ ; secondly,  $T$  values  $> 10$ , except if the modeling suggests the existence of a site from which the Fab dissociates below the level of detectability; thirdly, that the modeled kinetic parameters for the two sites are distinct; and fourthly, that the component  $S_m$  values are not highly distinct, i.e., that a minority site is not negligible in population size. The outcome was that meaningful heterogeneity was discernible within the population of BG505- but not the B41-trimer molecules that showed any detectable binding: for BG505, the  $\chi^2$

values were reduced 2.9- to 6.2-fold;  $T$  values were high except for a component of extremely slow dissociation of each Fab;  $k_{on1}/k_{on2}$  was 5.8 (PGT145) or 5.0 (PGT151) and  $k_{off1}/k_{off2}$  was  $> 200$  (PGT145) or  $> 76$  (PGT151);  $S_{m1}/S_{m2}$  was 1.0 (PGT145) or 1.7 (PGT151). The complex modeling also increased the stoichiometry for PGT145 from  $S_m = 0.74$  for Langmuir to a cumulative  $S_{m1} + S_{m2} = 0.92$  for heterogeneous-ligand modeling, a value close to the ideal  $S_m = 1.0$  (Table 2 and Additional file 1: Table S2).

In contrast, only the  $T$ -value criterion was met for the B41 trimer: the suggested kinetic constants and affinities were close or indistinguishable, and the minority populations small or negligible: specifically, for PGT151  $k_{on1}/k_{on2}$  was 1.2,  $k_{off1}/k_{off2}$  1.1,  $K_{D1}/K_{D2}$  0.82, and  $S_{m1}/S_{m2}$  110 (Additional file 1: Table S2): the sites did not differ tangibly in kinetics and the minority site was negligible.

In conclusion, two kinds of antigenic heterogeneity were detected: an *inclusive* kind, prevailing within the binding population of epitopes, was kinetically discernible for BG505; an *exclusive* kind, dividing the binding from the non-binding population, manifested itself as reduced stoichiometry for B41, very moderately for PGT145 but prominently for PGT151 binding to 2G12-purified trimer.

### Structural modeling of PGT151 binding to the B41 SOSIP.664 trimer

Using available structural data, we examined whether the differential PGT151 binding could be caused by pronounced conformational heterogeneity in B41 SOSIP.664 that would limit access to the PGT151 epitope (Fig. 8). As noted, we previously observed substantial conformational isomerism in B41 SOSIP.664 (Fig. 5, [25–27, 52]), as well as the ability of a CD4bs bNAb, b12, to bind to

**Table 2** Heterogeneous-ligand modeling<sup>a</sup>

SOSIP.664 Fab trimer	Affinity purification	$k_{on1}^b$ (1/Ms)	$k_{off1}^b$ (1/s)	$k_{on2}^b$ (1/Ms)	$k_{off2}^b$ (1/s)	$K_{D1}^b$ (nM)	$K_{D2}^b$ (nM)	$S_{m1}^b$	$S_{m2}^b$	$S_{m1}^b + S_{m2}^b$
BG505	PGT145 2G12 (n=3)	$2.9 \times 10^4 \pm 7.5 \times 10^2$	$< 10^{-5}$	$5.0 \times 10^3 \pm 7.0 \times 10^2$	$2.0 \times 10^{-3} \pm .1 \times 10^{-5}$	$< 0.5$	$4.1 \times 10^2 \pm 64$	$0.46 \pm 1.6 \times 10^{-2}$	$0.46 \pm 2.4 \times 10^{-2}$	$0.92 \pm 3.8 \times 10^{-2}$
	PGT151 2G12 (n=2)	$1.4 \times 10^5 \pm 1.3 \times 10^3$	$< 10^{-5}$	$2.8 \times 10^4 \pm 1.0 \times 10^3$	$7.6 \times 10^{-4} \pm 5 \times 10^{-5}$	$< 0.1$	$27 \pm 1.9$	$1.2 \pm 1.9 \times 10^{-2}$	$0.70 \pm 1.1 \times 10^{-2}$	$1.9 \pm 7.7 \times 10^{-3}$
B41	PGT145 2G12 (n=3)	$5.2 \times 10^4 \pm 1.4 \times 10^4$	$1.9 \times 10^{-4} \pm 3.6 \times 10^{-5}$	$1.6 \times 10^4 \pm 1.5 \times 10^3$	$1.1 \times 10^{-4} \pm .7 \times 10^{-5}$	$3.7 \pm 0.23$	$6.6 \pm 0.80$	$4.4 \times 10^{-2} \pm .4 \times 10^{-2}$	$0.59 \pm 3.6 \times 10^{-2}$	$0.63 \pm 1.8 \times 10^{-2}$
	PGT145 2G12 (n=3)	$3.5 \times 10^4 \pm 1.4 \times 10^4$	$< 10^{-5}$	$4.5 \times 10^4 \pm 1.1 \times 10^4$	$< 10^{-5}$	$< 0.5$	$< 0.5$	$0.13 \pm 0.13$	$0.74 \pm 0.16$	$0.87 \pm 5.1 \times 10^{-2}$
	PGT151 2G12 (n=2)	$3.1 \times 10^4 \pm 1.9 \times 10^3$	$8.5 \times 10^{-4} \pm 2.5 \times 10^{-4}$	$2.5 \times 10^4 \pm 5.5 \times 10^3$	$7.8 \times 10^{-4} \pm .8 \times 10^{-5}$	$28 \pm 9.8$	$34 \pm 12$	$0.45 \pm 2.9 \times 10^{-2}$	$4.1 \times 10^{-3} \pm 4.0 \times 10^{-3}$	$0.45 \pm 2.5 \times 10^{-2}$

<sup>a</sup>Tabulated values are means  $\pm$  S.E.M of *n* independent replicates<sup>b</sup>The constants and  $S_m$  are explained in Table 1 but here heterogeneous model allocates distinct values for two different sites, each indicated by the subscript 1 or 2.  $S_{m1} + S_{m2}$  = the cumulative stoichiometry

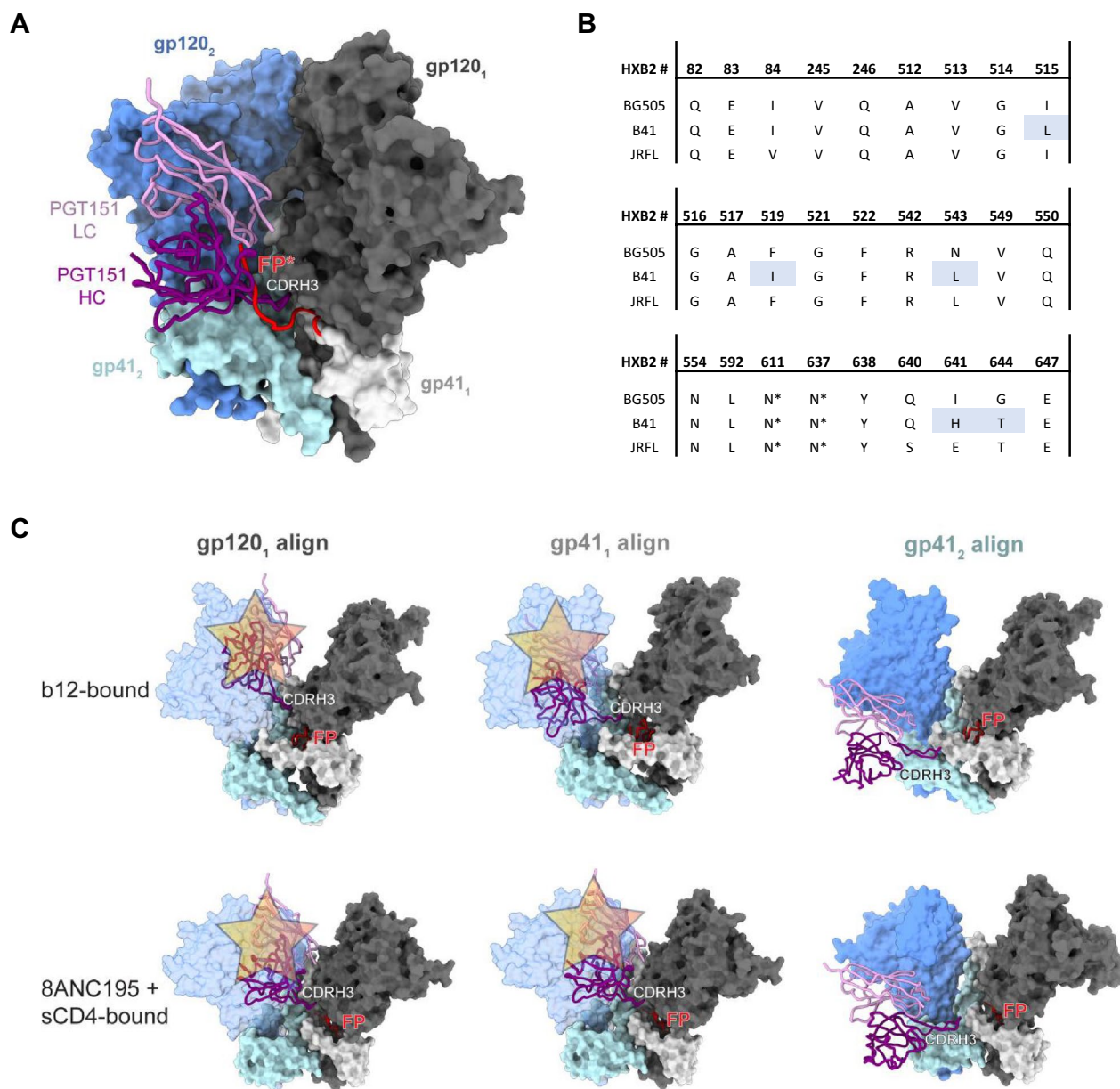


**Fig. 8** Structural constraints of PGT151 binding to B41 SOSIP.664. **A** PGT151 (PDB 5FUJ; in complex with JRFL Env [65]) aligned to a cryo-EM structure of B41 SOSIP.664 (PDB 6U59 [33]). The fusion peptide is depicted in red and derived from the PGT151 + JRFL SOSIP.664 [41] model for reference. **B** PGT151 contact residues in the epitope (as defined by  $< 4 \text{ \AA}$  distance from paratope atoms in the PGT151 + JRFL SOSIP.664 model) and equivalent positions in BG505 and B41 SOSIP.664 reveal high conservation. Amino acids different between B41 and BG505 are highlighted in light blue. **C** Alignment of PGT151 Fab from the PGT151 + JRFL SOSIP.664 structure onto the b12-bound (*top*, PDB 5VN8 [27]) or 8ANC195- and sCD4-bound (*bottom*, PDB 6EDU [29]) conformation using one of three reference chains [27, 29]. Note that for clarity, the b12, 8ANC195, and sCD4 structures have been removed from the reference model. Steric clashes are depicted with translucent buff-colored stars. The clashing gp120 subunit is depicted in transparent blue. For the rest, antibody and Env colors follow those in panel **A**

its conformationally dependent epitope on that trimer [27]. Earlier hydrogen–deuterium-exchange mass spectrometry (HDX-MS) experiments demonstrated that although b12 can bind BG505 SOSIP.664 trimers, it does so very slowly, and fails to neutralize the BG505

PV, suggesting that the required more open conformation is rarely sampled by BG505 SOSIP.664 and not triggered by the antibody in a timeframe conducive to neutralization [63]. Hence, the B41 trimer is intrinsically more flexible than the BG505 trimer (Figs. 5 and 8).

Double-electron–electron resonance (DEER) spectroscopy has revealed multiple conformations in the trimer base and inner domain of both BG505 and B41 SOSIP trimers, a flexibility that is uncoupled from that of the conformationally more fixed trimer apex [50]. Less conformational heterogeneity in the apex could explain the absence of marked PFs in PGT145 neutralization of either virus (Fig. 1). The same DEER experiments suggested a degree of conformational homogeneity in B41 SOSIP.v4.1, which includes stabilizing mutations to limit exposure of the V3 region and to shield non-NAb epitopes. But we did not study B41 SOSIP.v4.1 or other hyper-stabilized variants here, because we sought to mimic the neutralization-relevant conformational flexibility of Env on virions. We note, however, that the isomer conversion, accordingly, is quite plausibly limited by stabilizing mutations [50, 51]. The conformations of epitopes from apex to base are interconnected in a complex network of long- and short-range effects. For example, pre-binding of PGT145 to the BG505 SOSIP.664 trimer markedly reduces subsequent PGT151 binding, whereas no converse effect is detectable [64]. This non-reciprocal allosteric effect may not be identical for B41, but it suggests an intricate relationship between the two epitopes pertinent to the non-overlapping antigenicity maxima in the trimer population (Figs. 6 and 7; Tables 1 and 2; Additional file 1: Fig. S1).

The PGT151 epitope is unusually complex: PGT151 binding strictly depends on the native quaternary structure of proteolytically cleaved gp120-gp41 protomers. The paratope closely interacts with the interface between gp120 and gp41 of one protomer and glycans on both subunits of another protomer, inserting itself inter-protomerically [41] (Fig. 8A). Most residues implicated in the interaction are, however, identical for BG505 and B41, including the PNGSs at gp41 positions 611 and 637 (Fig. 8B). Both the fusion peptide (FP) and FP-proximate region (FPPR), reached by the inter-protomeric insertion of the long complementarity-determining region 3 of the heavy chain of the antibody, CDR H3, are highly similar in the two Envs (Fig. 8B). Modeling of PGT151 (based on a complex of its Fab with JR-FL SOSIP.664 [41]) onto a structure of closed-conformation B41 SOSIP.664 did not suggest any clashes or unfavorable interactions that would explain the different stoichiometries (Fig. 8C): the binding of two PGT151 Fabs was as unimpeded as in the structurally similar PGT151 Fab complexes with BG505 SOSIP.664 and membrane extracted, cytoplasmic-tail-truncated BG505 or JR-FL trimer analyzed by EM [41, 65]. Partially open, intermediate conformations of B41 SOSIP.664 have been solved by cryo-EM, including the aforementioned b12-bound state, one in complex with sCD4 and the interface-specific bNAb 8ANC195, and

a more rearranged sCD4- and 17b-bound one [27, 29]. Because conformational changes occur both in the gp120 and gp41 subunits in these states relative to the closed conformation, we aligned the PGT151-bound structure in three different ways for three parts of the epitope: to the part of the primary gp120 (gp120<sub>1</sub>), to the part of the primary gp41 (gp41<sub>1</sub>), which includes fusion-peptide residues, and to the component of the adjacent gp41 (gp41<sub>2</sub>) at its interface with the paratope (Fig. 8C). In the first two cases, the alignment to the primary subunit component of the epitope resulted in a clash of PGT151 with the adjacent gp120, which has rotated in response to b12 or sCD4 and 8ANC195 binding (Fig. 8C). This clash alone would prevent binding of PGT151 at this binding angle. Alignment to gp41<sub>2</sub> relieves the clash but allows paratope contacts with the trimer exclusively by the CDR H3, which is unlikely to yield tangible binding. Lastly, it was shown that, in the b12- or sCD4- and 17b-bound state, the fusion peptide of B41 SOSIP.664 is not solvent-accessible and is instead sequestered in a newly formed pocket in gp41 in all three protomers [27]. Sequestration of the fusion peptide may be a typical response to trimer opening, and this would remove a key component of the PGT151 epitope from the trimer.

In conclusion, the binding data suggest heterogeneity in how PGT145 and PGT151 recognize the total population of BG505 trimer, but that their binding is sufficient in strength and extent for the antibody to neutralize potently and effectively. Some subtler heterogeneity of PGT145 binding specifically to 2G12-purified B41 trimer was also apparent. Notably, however, the stark difference in stoichiometry of PGT151 binding to the BG505 and B41 trimers explains the larger PF of the B41 than of the BG505 neutralization. The low stoichiometry of PGT151 binding to B41 SOSIP.664 is explained, in turn, by reduced paratope access through steric hindrance and the sequestration of a key component of the epitope by the partial opening of the trimer, which the B41 SOSIP.664 trimer is prone to.

## Discussion

Studies on incomplete virus neutralization, which leaves distinct PFs, have a long history. Plateaus of maximum neutralization below 100% have been observed over time as the NAb association with virions progresses, or as the NAb concentration is increased. Multifarious explanations have been conjectured, but none has held up in general. Genetic resistance of the PF virus has been ruled out in several cases [4, 34–36, 66]. Arguably, both potency and efficacy are important in preventing viral acquisition in vivo. A meta-analysis showed that to protect 95% of macaques against SHIV acquisition, the serum 50%-inhibitory dilution factor, ID<sub>50</sub>, needed to

be  $\sim 700$  [46]. Provided the Hill coefficient of the sigmoid neutralization curve is equal to 1 [4, 67], and an asymptotic approach to 100% neutralization as in the meta-analysis, undiluted serum with that titer would neutralize 99.86% of an inoculum in vitro: a residual infectivity of 0.14% would translate into 5% failure to protect monkeys from acquisition. With the instantaneous inhibitory potentials that were determined in the meta-analysis, the in vitro neutralization required for protecting 95% of the monkeys was even higher,  $>99.9\%$ ; it was 93.7% for protection of 50% of the animals [46]. The meta-analysis comprised bNABs that were highly potent and effective against the challenge viruses and the assumptions within it are justified. In complementary analyses, we explored how reductions in efficacy and Hill coefficient affected the relationship between protection in vivo and neutralization in vitro, identifying conditions under which  $ID_{50}$  values  $\sim 700$  required for protection of 95% of the animals incidentally correspond to 95% neutralization in vitro (Additional file 1: Fig. S2A). But neutralization in vitro may differ in many respects from neutralization in vivo: the NAb concentrations in mucosae are considerably lower than in sera, more so in rectal than vaginal mucosa [68], and NAb potency may be lower in the setting of natural virus and target cells than in neutralization assays [4, 69–71]. We therefore also modeled how those factors under realistic assumptions would reduce the extrapolated  $ID_{50}$  values that pertain to neutralization in vivo and thereby eliminate the percentage gap between neutralization and protection (Additional file 1: Fig. S2B). Nevertheless, a PF of several percent, detectable in vitro, would arguably augur badly for protection from acquisition in vivo. The PF could also be larger in vivo than in vitro because of higher receptor density on target cells and greater spike density on virions [4, 69–71]. A large PF could thwart protection by preventive passive or active immunization. The importance of the PF in bNAB therapy may be even greater than in prevention, particularly when the aim is eradication: the viral swarm will be considerably more diversified antigenically than in the transmission bottleneck [72–74]. And heterogeneity of Env reduces the capacity of inhibitors to block viral entry [44].

We postulate variations in conformation and glycosylation, and combinations thereof, as potential sources of antigenic heterogeneity in clonal HIV-1 [27, 50, 65, 75–81]. The conformational heterogeneity could involve both glycans and peptidic segments, directly within the epitope and indirectly through distance effects. The heterogeneity at glycan sites could arise from variable occupancy and the precise glycan moiety. Specifically, the heterogeneity would have to be greater in B41 than

BG505 to explain the difference in PF in neutralization by PGT151.

Here we describe a PF of B41 neutralization by PGT151 of 21% and a negligible corresponding PF for BG505; PFs for both viruses were minor with PGT145. Incomplete neutralization by PGT151 is not restricted to B41: a range of 60–80% maximum neutralization was measured for 15% of PVs derived from 117 isolates, in contrast to 0.85% by PG9 (our calculations from [42]).

Also noteworthy is the stoichiometry of two PGT151 paratopes per trimer, the ligation of the first two epitopes apparently impeding that of the third [31, 41, 61]. The conformational changes restricting the stoichiometry may also stabilize the trimer [41]. Indeed, the mechanism of neutralization may be a block of the conformational changes induced by CD4 and the co-receptor in the absence of the bNAB [4, 5, 41, 82]. And the efficacy of that block may vary differently over trimer populations from different isolates.

The conformational plasticity of B41 Env [26, 27], combined with the allosteric interplay between the PGT145 and PGT151 epitopes, suggests a prominent conformational cause of the B41 PF with PGT151. Our findings of differential antigenicity after different purifications and depletions of B41 trimer, and of differential neutralization of B41 PV after depletion with either bNAB, are highly compatible with a conformational basis of the PF but do not exclude the influence of glycosylation. Glycan heterogeneity does not, however, confer variation in neutralization by all NABs: it is a hallmark of bNABs that they can make contacts with the N-acetyl-glucosamine (GlcNAc) stalk of the glycan, while avoiding clashes with high mannose and hybrid glycans of different sizes [39, 83].

We emphasize the possibility of different kinds of heterogeneity [84]: antigenically inclusive and exclusive, *i.e.*, modifying kinetics or stoichiometry. Within the population of the SOSIP trimer that does bind PGT145 or PGT151, we detected some heterogeneity by comparing Langmuir and heterogeneous-ligand modeling. The difference between the models was markedly clearer for BG505 than B41 (Tables 1 and 2 and Additional file 1: Tables S1 and S2). Two distinct sites with different kinetics and affinity of binding were discernable for BG505 for either bNAB. The combined stoichiometry, however, was high (0.92 and 1.9, respectively). If a similar heterogeneity exists on virion-associated Env spikes, these findings could signify that the higher-affinity site gets fully occupied at low concentrations of either bNAB, whereas additional partial occupancy on the lower-affinity site makes the sum sufficient for high efficacy of neutralization. Quite plausibly, affinity molds potency; stoichiometry determines efficacy.

What is the most plausible cause of the antigenic heterogeneity we have described here? If the antigenic heterogeneity had no basis in covalent differences, but purely consisted of conformers in equilibrium [85, 86], one might wonder why the same equilibrium is not re-established too rapidly after purifications and depletions to affect neutralization or binding by bNAbs. It may be noted, first, that non-equilibrium conformational dynamics can introduce differences in protein-molecule populations [87–89]. *Cis-trans* isomerization is catalyzed before the protein egresses from the cell and has been suggested to modify epitopes and paratopes, including HIV-1 bNAb paratopes [90–94]. Additionally, the protein molecules in solution and on PV particles, which accumulate extracellularly after egress from the secretory pathway and budding, span the ages from a few minutes to three days. Any age-related propensity for adopting different conformations could differ between Envs from distinct isolates, such as BG505 and B41.

Multiple covalent post-translational modifications of proteins, however, occur along the secretory pathway. Disulfide isomerization can create heterogeneity [95], but native-like Env trimers overwhelmingly converge to a uniform set of S–S bonds [96, 97]. Tyrosine sulfation in the V2 region of Env has been suggested to modulate neutralization sensitivity [98]. In the case of Env, however, the effect of differences in the extensive glycan shield are likely to dominate [75, 99–101]. The glycans that contact the PGT151 paratope [41], N611 and N637, have been described, respectively, as complex on both viral Env and tail-less trimers extracted by PGT151 from the viral envelope for both BG505 and B41 [102]. Antigenic effects of some mannose and underoccupancy on N611 of B41 SOSIP.664 and of some mannose on N637 of BG505 and B41 SOSIP.664 cannot be excluded but would not explain the PF since these glycans were all complex on virions [102–104]. Indirect effects of the multiple glycan differences at other sites seem more plausible [102].

To conclude, the multiple possibilities above notwithstanding, we favor the following causalities: differences in glycans between BG505 and B41 Env, and within the latter trimer population, stably confer distinct conformational propensities; B41 Env is thus more prone than BG505 Env to adopt a partially open conformation; the opening reduces the stoichiometry, because steric clashes would prevent PGT151 from binding; and the reduced stoichiometry, in turn, yields sub-neutralizing bNAb occupancy on Env and causes the PF (Fig. 8) [3, 4].

The glycosylation sites N156 and N160 are both crucial for neutralization by PGT145. N156, however, has indirect effects on the epitope; only the N160 glycan makes direct contact with the paratope [39]. The paratope interacts in an asymmetric manner, extensively with the N160

glycan on a first protomer, less so with the one on a second, and negligibly with the one on a third, the latter glycan projecting away from the paratope [39]. Again, the interaction is driven by the GlcNAc stalk: Man6, Man7, Man8, or hybrid moieties can be tolerated, but probably not bulkier complex glycans. Enough heterogeneity has been described for N160 to explain the observed heterogeneity in binding of the PGT145 Fab to the BG505 trimer: the glycan is partly processed but largely of oligomannose type [39, 102–104].

The stoichiometry of PGT145 Fab binding was close to the ideal 1.0 for both BG505 and B41. PGT151 binding also approached its described maximum stoichiometry of 2.0 on the BG505 trimer. In contrast, on the B41 trimer the PGT151 stoichiometry was a mere 0.45 after 2G12 purification, and the binding was barely detectable after PGT145 purification (Fig. 7, Table 1). A complete lack of binding to a large fraction of the trimer molecules explains the large PF for the B41-PGT151 combination. There is precedence for the association of a reduced stoichiometry with a large PF. The PF is 40% in PGT151 neutralization of the isolate IAVI C22, whereas a single PGT151 Fab binds to 60% of the IAVI C22 Env trimer. In contrast, two Fabs bind per BG505 and JR-FL trimer, and the corresponding viruses are neutralized to ~100% [41, 42]. But the proportion of sensitive virus cannot be directly derived from the stoichiometry: that proportion will be determined by the distribution of the antigenic forms of trimers on the virions combined with approximate thresholds of minimum occupancy for neutralization [69].

The binding of a bNAb may alter the conformational heterogeneity among the trimer molecules. But a large fraction of primarily non-antigenic Env epitopes that could be selected or induced to fit the paratope would conceivably not confer a large PF and would leave tell-tale marks on the SPR-curve shapes [31, 61, 105]. Less malleable antigenic heterogeneity is required to explain the PF. The occurrence of a fraction of non-inducible conformers also agrees with antigenic differences of sufficient stability not to be immediately eliminated by the resetting of equilibria after purifications and depletions, as discussed above.

The armamentarium of passive immunization offers straightforward remedies for large PFs caused by antigenic heterogeneity: combinations of bNAbs that have distinct preferences for glyco-forms or conformational variants of the antigen [49, 106, 107]. Do the results also inform active immunization? In cases of reciprocal enrichment and depletion of antigenic forms by affinity purification with certain antibodies, such as PGT145 and PGT151, the immune responses might be skewed towards resembling the antibody used for purification

of the immunogen. But elicitation of responses to apical and interface bNAb epitopes are still not readily achieved by immunogens purified with these bNAbs. The goal of eliciting responses to multiple bNAb epitopes, however, might still be favored by immunogens purified with bNAbs such as 2G12 that largely do not segregate distinct antigenic forms of the immunogen or by combinations of differentially purified immunogen.

To elicit bNAbs, it may be crucial to avoid other, potentially distracting responses, such as narrowly active autologous NAb. B41-autologous NAb tend to target the lining of holes in the glycan shield around residues N230 and N289 [21, 33]. Such epitopes, targeted by the rabbit mono- and polyclonal antibodies we studied here, were less exposed on the PGT151- than the PGT145-purified trimer. These rabbit antibodies neutralized PGT151-depleted PV more potently and effectively than PGT145-depleted PV. PGT151 purification also reduced PGT145 binding specifically to the B41 SOSIP.664 trimer much less than vice versa. Those skewed specificities would suggest advantages to PGT151- over PGT145-purified immunogen. But inducing bNAbs that leave as large a PF as PGT151 does against many isolates would not be optimal [42]. Therefore again, combinations of antigenic variants may be more conducive to rendering responses broader and more effective.

We conclude that antigenic heterogeneity within genetically homogeneous Env-protein populations can differ drastically among HIV-1 strains, which is directly exemplified here and in line with data on multiple isolates [42]. The ensuing effects on neutralization efficacy and potency can be strong. Countermeasures can be designed both in passive and active immunization. In the latter case, the heterogeneity may even be harnessed in the pursuit of breadth.

## Methods

### Aim, design, and setting

The aim of this study was to find explanations for reduced efficacy in HIV-1 neutralization. We compared the neutralization of the Clade A BG505 isolate with that of Clade B B41 by three bNAbs, 2G12, PGT145, and PGT151, as well as post-immunization rabbit poly- and monoclonal antibodies. We observed large PFs specifically with B41 and PGT151 and the rabbit antibodies. We dissected the heterogeneity by performing neutralization of bNAb- or mock-depleted PV and studies of bNAb binding to bNAb-purified SOSIP trimers by ELISA and SPR. We correlated the findings with available protein-structural and glycosylation data.

### Antibodies and sera

The human bNAbs VRC01, 2G12, PGT121, and PGT145 [38–40, 108] were obtained from the International AIDS Vaccine Initiative (IAVI, La Jolla), VRC34.01 [54] from John Mascola (VRC, NIH), 35O22 [109] from Mark Connors (VRC, NIH). The bNAb 3BC315 was produced by us, as described [58].

Rabbit sera collected after three immunizations with B41 SOSIP.664 (animal numbers 5713, 5714, and 5716) were chosen from a group of five; one other serum showed poor neutralization and another serum undetectable PF [32]. All five sera in a group obtained after three immunizations with B41 SOSIP.v4.1 in a separate experiment showed potent neutralization with detectable PFs of varied sizes; all five of these sera were included [18]. The rabbit mNAbs 13A and 16D were provided by Marit J van Gils (AMC). They were isolated from rabbits 5713 and 5716, respectively, and are among the most potent lineage members of all of six lineages from these rabbits.

PGT145- and PGT151-Fab plasmids were expressed and purified as described previously [61]. Briefly, HEK 293F suspension cells were transiently transfected with Fab plasmids. Fabs were initially purified on anti-human affinity column (kappa XL matrix). Fabs were further subjected to ion-exchange fractionation by AKTA FPLC to remove dimers of light chains. The purity of the Fabs was confirmed on SDS PAGE gel (reducing and non-reducing) before binding analyses.

### Pseudo-virus production

HEK-293 T cells were transfected with HIV-1 BG505 and B41 *env* and luciferase-reporter plasmids [25, 110, 111] to produce pseudo-virus (PV). B41 Env for the PV has an R315Q mutation in the V3 region to make it similar to B41 SOSIP.664, which has the substitution to prevent proteolytic clipping [26]. One day before transfection, cells maintained in growth medium (DMEM with 10% FBS, 2 mM L-Glutamine and 1% Pen-Strep) were seeded in 6-well plates at a density of  $4 \times 10^5$  cells per well. From 3 h before transfection 50–60%-confluent cell cultures were maintained in antibiotic-free growth medium. The HIV-1 BG505 or B41 *env* in pCDNA3 and pNL4.1AM $\Delta env \Delta vpr + luc$  plasmids [25, 110] at a ratio of 1:2 were mixed with the Effectene Transfection Reagent (Qiagen) and the mix was added to the cultures, which were incubated at 37 °C with 5% CO<sub>2</sub>. The next day, cells were supplemented with fresh growth medium. 48 h thereafter, PV-containing supernatants were harvested and spun at 2000 rpm for 10 min. Additional FBS to a total of 20% was added to the supernatant, before spinning, to avoid virion degradation.

### TZM-bl neutralization assay

The persistent fraction of infectivity after neutralization of BG505 and B41 PV was measured, and the neutralization of PGT145-, PGT151-, and mock-depleted B41 PV (see below) was compared in a neutralization assay based on TZM-bl cells [112]. Initially in this study, neutralization assays were performed as described previously [25, 110]. Subsequently, after a lab-routine switch during the pandemic, we used a slightly different TZM-bl-PV system [111], yielding indistinguishable results. Briefly, the day before infection, cells were seeded in 96-well plates (white tissue-culture treated, Costar 3917), at a density of  $1 \times 10^4$  cells per well. PV at a dose yielding luminescence readouts of  $\sim 2 \times 10^6$  counts per second was incubated for 1 h at 37 °C with 5% CO<sub>2</sub> with select bNAb or heat-inactivated serum samples, all serially diluted in DMEM growth medium. The reason for the high dose is that it gives a wide dynamic range, amenable to sensitive PF identification. It was verified that it gives zero bleed-through of signal to neighboring wells. 50 µl mix or medium only (cell control) was then transferred to TZM-bl cells seeded the night before (4 replicates) in wells with 50 µl medium or to wells with 50 µl medium without cells (viral-input control, 2 replicates), all wells containing 15 µg/ml DEAE-Dextran. Two days later, the medium was carefully aspirated and the cells were lysed with Glo-lysis buffer (Promega E153A) during 15 min on a shaker. 25 µl Nano-Glo Dual-Luciferase substrate (Promega 1610) was added to each well. Luciferase-generated signal was read with an Enspire multimode plate reader (Perkin Elmer). Data were processed by subtracting the background signals of cell- and virus-only from sample wells. Virus incubated without antibody was considered to give 100% infectivity and percent inhibition was calculated for all samples.

In a variation of the standard set-up, serially diluted PV was instead incubated with a constant concentration of antibody (50 µg/ml) or with medium for 1 h at 37°. The PV-bNAb mix was added to the Tzm-bl cells, and the cultures continued; on day 2 post-infection, cells were washed and lysed, and signals generated and measured as above. Neutralization data were plotted and analyzed with GraphPad Prism 6 software.

### Depletion of PV with bNAbs

Supernatants with PV were added to columns containing Sepharose 4B beads with CNBr-coupled PGT145, PGT151, or no antibody (as mock control). PV mixed with beads were incubated at 37 °C with 5% CO<sub>2</sub> for 3 h on a nutator. After 3 h, beads were allowed to settle down at room temperature. PV was collected by gravity flow from the respective column, filtered through 0.45 µm membranes, concentrated by Vivaspin columns with a

100-kDa cut off (Cytiva), and immediately tested in the neutralization assay.

### Expression, purification, and fractionation of SOSIP trimers

BG505 and B41 SOSIP.664-His genes were cloned into the pPPI4 expression vector (GenScript). Expi-293F cells were transiently transfected by FectoPRO (VWR). Cells were seeded at a density of  $4 \times 10^6$  cells/ml in 250 ml of medium with  $1 \times$  penicillin–streptomycin (Corning) one day before transfection. On the day of transfection, cells with 90% viability were suspended in antibiotic-free medium at  $6 \times 10^6$  cells/ml. For transfection, HIV-1 *env* and *furin* plasmids were diluted in Optimum at a ratio of 4:1, mixed with FectoPRO reagent, and incubated at room temperature for 10 min. The FectoPRO-DNA mix and FectoPRO Booster were added to the cells. Transfected cells were incubated at 37 °C with 5% CO<sub>2</sub> and continuous shaking for 3 days. After 3 days, cells were centrifuged at 3000 rpm for 30 min. Supernatant was collected and passed through a 0.2-µm filter.

Filtered supernatant was first passed through a 2G12-, PGT145-, or PGT151-affinity column. Affinity columns were made by cross-linking bNAbs to activated CNBr Sepharose 4B beads (GE Healthcare). Bound trimer was eluted with 3 M MgCl<sub>2</sub>, which was then removed by dialyzing through snake-skin tubing in an exchange buffer (TN150: 20 mM Tris–HCl, 150 mM NaCl, pH 8) overnight at 4 °C. Further purification of the 2G12-purified trimer was done by size-exclusion chromatography (SEC) on a HiLoad 16/600 Superdex 250 preparative-grade column with TN150 as running buffer to remove aggregates, dimers, and monomers. TN150 was used as running buffer during SEC. Protein concentrations were determined by the bicinchoninic assay (BCA). Trimer content in SEC fractions was assessed by Blue Native-PAGE; pure trimer fractions were pooled and stored at – 80 °C till further analysis by NS-EM.

2G12- and PGT145-affinity purifications followed by SEC have been shown multiple times by negative-stain electron microscopy (NS-EM) to give BG505 and B41 SOSIP.664 trimers with nearly exclusively native-like structure [18, 23–26, 31, 51]. Here we confirmed by the same method, performed as previously described [25], that PGT151 purification of B41 SOSIP.664 trimer also gave 100% native-like trimer (see Results and Fig. 5).

The BG505 and B41 SOSIP.664 trimers were also affinity-purified for antigenic analyses (Figs. 6, 7, Tables 1 and 2, Additional file 1: Fig. S1, Tables S1 and S2). Briefly, supernatant from the 293-transfection cultures was collected, passed through a 0.2-µm filter, and then through 2G12-, PGT145-, and PGT151-affinity columns. Bound trimer was eluted with 3 M MgCl<sub>2</sub>, which was removed

as above. SEC was then performed and trimer fractions identified and stored as above.

In addition, a portion of the 2G12-SEC-purified B41 SOSIP.664 trimer was PGT145- and PGT151-depleted. The trimer was resuspended in TN150 buffer and incubated in PGT145-, PGT151-, or mock-affinity columns at room temperature for 2 h, with constant nutating. After 2 h, the unbound, depleted fraction of trimer was allowed to flow through the column. Effluent was collected and concentrated on Viva Spin columns. The quality and purity of all fractions were checked by BN-PAGE and the protein concentration determined by the bicinchoninic acid assay.

### Analysis of antibody binding by ELISA

Lectin-capture ELISA for analyzing antibody binding to Env SOSIP trimers has been previously described [62]. It was chosen here because of poor immobilization of the His-tagged trimer to Ni<sup>2+</sup> plates. 96-well plates were coated with GNL-lectin (Sigma) at 5 µg/ml in 100 µl per well by overnight incubation. All steps were performed at room temperature. The next day, wells were washed once with Tris-buffered saline (TBS) and blocked for 1 h with 10% FBS and 1% skimmed milk in 200 µl TBS. The plates were then washed twice with TBS and B41 SOSIP.664 trimer at 2 µg/ml was captured by the lectin for 2 h. The plates were washed twice and antibody serially diluted in TBS with 5% FBS and 1% skimmed milk was added. After 1 h, the plates were washed thrice with TBS. Then goat anti-human-HRP or anti-rabbit-HRP conjugate was added. After 45 min, the plates were washed four times with TBS containing 0.05% tween-20. Then 3,3',5,5'-tetramethylbenzidine (TMB) was added for 2–5 min and finally 0.3 M HCl to stop the reaction. The OD was recorded at 450 nm.

### Analysis of antibody binding by surface plasmon resonance

Antibody binding to purified and fractionated SOSIP.664 trimers was also analyzed by SPR on BIACore 3000 and T200 instruments at 25 °C [31]. Briefly, trimers were immobilized to  $R_L$  values close to 250 response units (RU) by anti-His antibody that had been covalently coupled to a CM5 sensor chip as described [61, 105]. In each cycle, fresh Env protein was captured, and at the end of each cycle, Env trimer was removed by a pulse of 10 mM glycine (pH 2.0) for one minute at a flow rate of 30 µl min<sup>-1</sup>. IgG of bNAbs at a concentration of 500 nM was injected for 300 s of association and 600 s of dissociation. For full kinetic analysis, Fabs of PGT145 and PGT151 were titrated down from 1 µM in

twofold steps till absence of detectable signal. Significant mass-transfer limitation was prevented by a high flow rate (50 µl/min); its absence was confirmed by  $k_t$  analysis. Binding data were analyzed with BIAevaluation software. Data from Fab titrations were fitted to Langmuir and heterogeneous-ligand models. The binding of PGT151 Fab to 2G12-purified B41 SOSIP was modeled with baseline drift ( $2-7 \times 10^{-3}$  RU/s) because of slight trimer dissociation from anti-His-capture antibody. The modeling was validated by calculations of  $\chi^2$  for the overall fit and  $T$  values for the individual fitted parameters (Additional file 1: Tables S1 and S2).

### Supplementary Information

The online version contains supplementary material available at <https://doi.org/10.1186/s12977-023-00624-9>.

**Additional file 1: Table S1.** Validation of Langmuir modeling. **Table S2.** Validation of heterogeneous-ligand modeling. **Figure S1.** Analysis of bNAb binding to differentially bNAb-purified B41 SOSIP.664 by ELISA. Each diagram shows the binding of one bNAb to BG505 or B41 SOSIP.664 trimers purified in three ways. The optical densities are plotted on the y axes as functions of the bNAb concentrations. **Figure S2.** Extent of neutralization in vitro as a predictor of protection in vivo.

### Acknowledgements

The following reagent was obtained through the NIH HIV Reagent Program, Division of AIDS, NIAID, NIH: Human Immunodeficiency Virus Type 1 (HIV-1) SG3ΔEnv Non-infectious Molecular Clone, ARP-11051 and Tzm-bl cells [112], ARP-8129, were contributed by Drs. John C. Kappes and Xiaoyun Wu and Tranzyme Inc. The pHIV-1<sub>NL4-3</sub> ΔEnv-NanoLuc plasmid was gratefully obtained from Paul Bieniasz. We are grateful to Randy Diaz-Tapia and Oscar Feliciano for expert technical assistance.

### Author contributions

PC and RPR performed virus depletion and neutralization experiments; TJK carried out complementary neutralization assays; AY performed SPR analyses; GO and WHL performed NS-EM; GO modeled molecular structures and interactions; ABW advised on the structural work; JPM provided funding and advice; PJK designed the experiments together with PC, RPR, and AY and wrote the manuscript, which PC, RPR, GO, JPM, and PJK edited. All authors read and approved the final manuscript.

### Funding

This work was supported by R01 AI036082 (JPM and PJK).

### Availability of data and materials

All relevant data are contained in the article including its supplementary information; Protein Databank Coordinates for previously published structural data that were used are provided in the legend to Fig. 8 (PDB 5FUU, PDB 6U59, PDB 5VN8, and PDB 6EDU).

### Declarations

#### Ethics approval and consent to participate

Not applicable.

#### Consent for publication

Not applicable.

#### Competing interests

The authors declare that they have no competing interests.

**Author details**

<sup>1</sup>Department of Microbiology and Immunology, Weill Cornell Medicine, Cornell University, 1300 York Avenue, 62, New York, NY 10065, USA. <sup>2</sup>Department of Integrative Structural and Computational Biology, Consortium for HIV Vaccine 14 Development (CHAVID), The Scripps Research Institute, La Jolla, CA 92037, USA. <sup>3</sup>Present Address: Toulouse Institute for Infectious and Inflammatory Diseases, Infinity, Université de Toulouse, CNRS, INSERM, UPS, Toulouse, France. <sup>4</sup>Present Address: Virology Unit, Institute of Microbial Technology, Council of Scientific and Industrial Research (CSIR), Chandigarh, India.

Received: 21 February 2023 Accepted: 15 May 2023

Published online: 27 May 2023

**References**

- Burton DR. Antibodies, viruses and vaccines. *Nat Rev Immunol.* 2002;2:706–13.
- Plotkin SA. Correlates of protection induced by vaccination. *Clin Vaccine Immunol.* 2010;17:1055–65.
- Burton DR. Antiviral neutralizing antibodies: from in vitro to in vivo activity. *Nat Rev Immunol.* 2023. <https://doi.org/10.1038/s41577-023-00858-w>.
- Klasse PJ. Neutralization of virus infectivity by antibodies: old problems in new perspectives. *Adv Biol.* 2014;2014:157895.
- Burton DR, Saphire EO, Parren PW. A model for neutralization of viruses based on antibody coating of the virion surface. *Curr Top Microbiol Immunol.* 2001;260:109–43.
- Burton DR. What are the most powerful immunogen design vaccine strategies? Reverse vaccinology 2.0 shows great promise. *Cold Spring Harb Perspect Biol.* 2017;9:a030262.
- Burton DR. Advancing an HIV vaccine; advancing vaccinology. *Nat Rev Immunol.* 2019;19:77–8.
- Burton DR, Hangartner L. Broadly neutralizing antibodies to HIV and their role in vaccine design. *Annu Rev Immunol.* 2016;34:635–59.
- Escolano A, Dosenovic P, Nussenzweig MC. Progress toward active or passive HIV-1 vaccination. *J Exp Med.* 2017;214:3–16.
- Haynes BF, Wiehe K, Borrow P, Saunders KO, Korber B, Wagh K, McMichael AJ, Kelsoe G, Hahn BH, Alt F, Shaw GM. Strategies for HIV-1 vaccines that induce broadly neutralizing antibodies. *Nat Rev Immunol.* 2022. <https://doi.org/10.1038/s41577-022-00753-w>.
- Kwong PD, Mascola JR. HIV-1 vaccines based on antibody identification, B cell ontogeny, and epitope structure. *Immunity.* 2018;48:855–71.
- Kwong PD, Mascola JR, Nabel GJ. Broadly neutralizing antibodies and the search for an HIV-1 vaccine: the end of the beginning. *Nat Rev Immunol.* 2013;13:693–701.
- Klasse PJ, Ozorowski G, Sanders RW, Moore JP. Env exceptionalism: why are HIV-1 Env glycoproteins atypical immunogens? *Cell Host Microbe.* 2020;27:507–18.
- Klein F, Mouquet H, Dosenovic P, Scheid JF, Scharf L, Nussenzweig MC. Antibodies in HIV-1 vaccine development and therapy. *Science.* 2013;341:1199–204.
- West AP Jr, Scharf L, Scheid JF, Klein F, Bjorkman PJ, Nussenzweig MC. Structural insights on the role of antibodies in HIV-1 vaccine and therapy. *Cell.* 2014;156:633–48.
- Chen X, Zhou T, Schmidt SD, Duan H, Cheng C, Chuang GY, Gu Y, Louder MK, Lin BC, Shen CH, et al. Vaccination induces maturation in a mouse model of diverse unmutated VRC01-class precursors to HIV-neutralizing antibodies with > 50% breadth. *Immunity.* 2021;54:324–339.e328.
- Escolano A, Gristick HB, Gautam R, DeLaisch AT, Abernathy ME, Yang Z, Wang H, Hoffmann MAG, Nishimura Y, Wang Z, et al. Sequential immunization of macaques elicits heterologous neutralizing antibodies targeting the V3-glycan patch of HIV-1 Env. *Sci Transl Med.* 2021;13:1533.
- Ringe RP, Pugach P, Cottrell CA, LaBranche CC, Seabright GE, Ketas TJ, Ozorowski G, Kumar S, Schorcht A, van Gils MJ, et al. Closing and opening holes in the glycan shield of HIV-1 envelope glycoprotein SOSIP trimers can redirect the neutralizing antibody response to the newly unmasked epitopes. *J Virol.* 2019;93:e01656–18.
- Schorcht A, Cottrell CA, Pugach P, Ringe RP, Han AX, Allen JD, van den Kerkhof T, Seabright GE, Schermer EE, Ketas TJ, et al. The glycan hole area of HIV-1 envelope trimers contributes prominently to the induction of autologous neutralization. *J Virol.* 2022;96:e0155221.
- Zhang P, Narayanan E, Liu Q, Tsybovsky Y, Boswell K, Ding S, Hu Z, Follmann D, Lin Y, Miao H, et al. A multiclade env-gag VLP mRNA vaccine elicits tier-2 HIV-1-neutralizing antibodies and reduces the risk of heterologous SHIV infection in macaques. *Nat Med.* 2021;27:2234–45.
- Klasse PJ, Ketas TJ, Cottrell CA, Ozorowski G, Debnath G, Camara D, Francomano E, Pugach P, Ringe RP, LaBranche CC, et al. Epitopes for neutralizing antibodies induced by HIV-1 envelope glycoprotein BG505 SOSIP trimers in rabbits and macaques. *PLoS Pathog.* 2018;14:e1006913.
- Derking R, Allen JD, Cottrell CA, Sliepen K, Seabright GE, Lee WH, Aldon Y, Rantalainen K, Antanasijevic A, Copps J, et al. Enhancing glycan occupancy of soluble HIV-1 envelope trimers to mimic the native viral spike. *Cell Rep.* 2021;35:108933.
- Julien JP, Cupo A, Sok D, Stanfield RL, Lyumkis D, Deller MC, Klasse PJ, Burton DR, Sanders RW, Moore JP, et al. Crystal structure of a soluble cleaved HIV-1 envelope trimer. *Science.* 2013;342:1477–83.
- Lyumkis D, Julien JP, de Val N, Cupo A, Potter CS, Klasse PJ, Burton DR, Sanders RW, Moore JP, Carragher B, et al. Cryo-EM structure of a fully glycosylated soluble cleaved HIV-1 envelope trimer. *Science.* 2013;342:1484–90.
- Sanders RW, Derking R, Cupo A, Julien JP, Yasmeen A, de Val N, Kim HJ, Blattner C, de la Pena AT, Korzun J, et al. A next-generation cleaved, soluble HIV-1 Env trimer, BG505 SOSIP.664 gp140, expresses multiple epitopes for broadly neutralizing but not non-neutralizing antibodies. *PLoS Pathog.* 2013;9:e1003618.
- Pugach P, Ozorowski G, Cupo A, Ringe R, Yasmeen A, de Val N, Derking R, Kim HJ, Korzun J, Golabek M, et al. A native-like SOSIP.664 trimer based on an HIV-1 subtype B env gene. *J Virol.* 2015;89:3380–95.
- Ozorowski G, Pallesen J, de Val N, Lyumkis D, Cottrell CA, Torres JL, Copps J, Stanfield RL, Cupo A, Pugach P, et al. Open and closed structures reveal allosteric and pliability in the HIV-1 envelope spike. *Nature.* 2017;547:360–3.
- Pancera M, Zhou T, Druz A, Georgiev IS, Soto C, Gorman J, Huang J, Acharya P, Chuang GY, Ofek G, et al. Structure and immune recognition of trimeric pre-fusion HIV-1 Env. *Nature.* 2014;514:455–61.
- Wang H, Barnes CO, Yang Z, Nussenzweig MC, Bjorkman PJ. Partially open HIV-1 envelope structures exhibit conformational changes relevant for coreceptor binding and fusion. *Cell Host Microbe.* 2018;24:579–592.e574.
- Schommers P, Gruell H, Abernathy ME, Tran MK, Dingens AS, Gristick HB, Barnes CO, Schoofs T, Schlotz M, Vanshilla K, et al. Restriction of HIV-1 escape by a highly broad and potent neutralizing antibody. *Cell.* 2020;180:471–489.e422.
- Yasmeen A, Ringe R, Derking R, Cupo A, Julien JP, Burton DR, Ward AB, Wilson IA, Sanders RW, Moore JP, Klasse PJ. Differential binding of neutralizing and non-neutralizing antibodies to native-like soluble HIV-1 Env trimers, uncleaved Env proteins, and monomeric subunits. *Retrovirology.* 2014;11:41.
- Klasse PJ, LaBranche CC, Ketas TJ, Ozorowski G, Cupo A, Pugach P, Ringe RP, Golabek M, van Gils MJ, Guttman M, et al. Sequential and simultaneous immunization of rabbits with HIV-1 envelope glycoprotein SOSIP.664 trimers from clades A, B and C. *PLoS Pathog.* 2016;12:e1005864.
- Yang YR, McCoy LE, van Gils MJ, Andrabi R, Turner HL, Yuan M, Cottrell CA, Ozorowski G, Voss J, Pauthner M, et al. Autologous antibody responses to an HIV envelope glycan hole are not easily broadened in rabbits. *J Virol.* 2020;94:e01861–19.
- Burnet FM, Keogh EV, Lush D. The immunological reactions of the filterable viruses. *Aust J Exp Biol Med Sci.* 1937;15:227–368.
- Dulbecco R, Vogt M, Strickland AG. A study of the basic aspects of neutralization of two animal viruses, western equine encephalitis virus and poliomyelitis virus. *Virology.* 1956;2:162–205.
- Mandel B. Neutralization of animal viruses. *Adv Virus Res.* 1978;23:205–68.
- McCoy LE, Falkowska E, Doores KJ, Le K, Sok D, van Gils MJ, Euler Z, Burger JA, Seaman MS, Sanders RW, et al. Incomplete neutralization and deviation from sigmoidal neutralization curves for HIV broadly neutralizing monoclonal antibodies. *PLoS Pathog.* 2015;11:e1005110.
- Trkola A, Purtscher M, Muster T, Ballaun C, Buchacher A, Sullivan N, Srinivasan K, Sodroski J, Moore JP, Katinger H. Human monoclonal

- antibody 2G12 defines a distinctive neutralization epitope on the gp120 glycoprotein of human immunodeficiency virus type 1. *J Virol*. 1996;70:1100–8.
39. Lee JH, Andrabi R, Su CY, Yasmeen A, Julien JP, Kong L, Wu NC, McBride R, Sok D, Pauthner M, et al. A broadly neutralizing antibody targets the dynamic HIV envelope trimer apex via a long, rigidified, and anionic beta-hairpin structure. *Immunity*. 2017;46:690–702.
  40. Walker LM, Huber M, Doores KJ, Falkowska E, Pejchal R, Julien JP, Wang SK, Ramos A, Chan-Hui PY, Moyle M, et al. Broad neutralization coverage of HIV by multiple highly potent antibodies. *Nature*. 2011;477:466–70.
  41. Blattner C, Lee JH, Sliepen K, Derking R, Falkowska E, de la Pena AT, Cupo A, Julien JP, van Gils M, Lee PS, et al. Structural delineation of a quaternary, cleavage-dependent epitope at the gp41-gp120 interface on intact HIV-1 Env trimers. *Immunity*. 2014;40:669–80.
  42. Falkowska E, Le KM, Ramos A, Doores KJ, Lee JH, Blattner C, Ramirez A, Derking R, van Gils MJ, Liang CH, et al. Broadly neutralizing HIV antibodies define a glycan-dependent epitope on the prefusion conformation of gp41 on cleaved envelope trimers. *Immunity*. 2014;40:657–68.
  43. Wu X, Parast AB, Richardson BA, Nduati R, John-Stewart G, Mbori-Ngacha D, Rainwater S, Overbaugh J. Neutralization escape variants of human immunodeficiency virus type 1 are transmitted from mother to infant. *J Virol*. 2006;80:835–44.
  44. Ketas TJ, Holuigue S, Matthews K, Moore JP, Klasse PJ. Env-glycoprotein heterogeneity as a source of apparent synergy and enhanced cooperativity in inhibition of HIV-1 infection by neutralizing antibodies and entry inhibitors. *Virology*. 2012;422:22–36.
  45. Gristick HB, Hartweg H, Loewe M, van Schooten J, Ramos V, Oliveira TY, Nishimura Y, Koranda NS, Wall A, Yao KH, et al. CD4 binding site immunogens elicit heterologous anti-HIV-1 neutralizing antibodies in transgenic and wild-type animals. *Sci Immunol*. 2023;8:eade6364.
  46. Pegu A, Borate B, Huang Y, Pauthner MG, Hessel AJ, Julg B, Doria-Rose NA, Schmidt SD, Carpp LN, Cully MD, et al. A meta-analysis of passive immunization studies shows that serum-neutralizing antibody titer associates with protection against SHIV challenge. *Cell Host Microbe*. 2019;26:336–346.e333.
  47. Caskey M, Klein F, Nussenzweig MC. Broadly neutralizing anti-HIV-1 monoclonal antibodies in the clinic. *Nat Med*. 2019;25:547–53.
  48. Haynes BF, Burton DR, Mascola JR. Multiple roles for HIV broadly neutralizing antibodies. *Sci Transl Med*. 2019;11:eaaz2686.
  49. LaMont C, Otwinowski J, Vanshilla K, Gruell H, Klein F, Nourmohammad A. Design of an optimal combination therapy with broadly neutralizing antibodies to suppress HIV-1. *Elife*. 2022;11:e76004.
  50. Stadtmueller BM, Bridges MD, Dam KM, Lerch MT, Huey-Tubman KE, Hubbell WL, Bjorkman PJ. DEER Spectroscopy measurements reveal multiple conformations of HIV-1 SOSIP envelopes that show similarities with envelopes on native virions. *Immunity*. 2018;49:235–246.e234.
  51. de Taeye SW, Ozorowski G, de la Torrents Pena A, Guttman M, Julien JP, van den Kerkhof TL, Burger JA, Pritchard LK, Pugach P, Yasmeen A, et al. Immunogenicity of stabilized HIV-1 envelope trimers with reduced exposure of non-neutralizing epitopes. *Cell*. 2015;163:1702–15.
  52. Kumar S, Sarkar A, Pugach P, Sanders RW, Moore JP, Ward AB, Wilson IA. Capturing the inherent structural dynamics of the HIV-1 envelope glycoprotein fusion peptide. *Nat Commun*. 2019;10:763.
  53. Andrewes CH, Elford WJ. Observations on anti-phage sera. I: "The percentage law." *Br J Exp Pathol*. 1933;XIV:368–76.
  54. Kong R, Xu K, Zhou T, Acharya P, Lemmin T, Liu K, Ozorowski G, Soto C, Taft JD, Bailer RT, et al. Fusion peptide of HIV-1 as a site of vulnerability to neutralizing antibody. *Science*. 2016;352:828–33.
  55. Ringe RP, Cruz Portillo VM, Dosenovic P, Ketas TJ, Ozorowski G, Nogal B, Perez L, LaBranche CC, Lim J, Francomano E, et al. Neutralizing antibody induction by HIV-1 Envelope glycoprotein SOSIP trimers on iron oxide nanoparticles may be impaired by mannose binding lectin. *J Virol*. 2020;94:e01883–19.
  56. Ringe RP, Sanders RW, Yasmeen A, Kim HJ, Lee JH, Cupo A, Korzun J, Derking R, van Montfort T, Julien JP, et al. Cleavage strongly influences whether soluble HIV-1 envelope glycoprotein trimers adopt a native-like conformation. *Proc Natl Acad Sci USA*. 2013;110:18256–61.
  57. Huang J, Kang BH, Pancera M, Lee JH, Tong T, Feng Y, Imamichi H, Georgiev IS, Chuang GY, Druz A, et al. Broad and potent HIV-1 neutralization by a human antibody that binds the gp41-gp120 interface. *Nature*. 2014;515:138–42.
  58. Lee JH, Leaman DP, Kim AS, de la Torrents Pena A, Sliepen K, Yasmeen A, Derking R, Ramos A, de Taeye SW, Ozorowski G, et al. Antibodies to a conformational epitope on gp41 neutralize HIV-1 by destabilizing the Env spike. *Nat Commun*. 2015;6:8167.
  59. Klein JS, Bjorkman PJ. Few and far between: how HIV may be evading antibody avidity. *PLoS Pathog*. 2010;6:e1000908.
  60. Klein JS, Gnanapragasam PN, Galimidi RP, Foglesong CP, West AP Jr, Bjorkman PJ. Examination of the contributions of size and avidity to the neutralization mechanisms of the anti-HIV antibodies b12 and 4E10. *Proc Natl Acad Sci USA*. 2009;106:7385–90.
  61. Brouwer PJM, Antanasijevic A, Berndsen Z, Yasmeen A, Fiala B, Bijl TPL, Bontjer I, Bale JB, Sheffler W, Allen JD, et al. Enhancing and shaping the immunogenicity of native-like HIV-1 envelope trimers with a two-component protein nanoparticle. *Nat Commun*. 2019;10:4272.
  62. Brouwer PJM, Antanasijevic A, de Gast M, Allen JD, Bijl TPL, Yasmeen A, Ravichandran R, Burger JA, Ozorowski G, Torres JL, et al. Immunofocusing and enhancing autologous Tier-2 HIV-1 neutralization by displaying Env trimers on two-component protein nanoparticles. *NPJ Vaccines*. 2021;6:24.
  63. Guttman M, Cupo A, Julien JP, Sanders RW, Wilson IA, Moore JP, Lee KK. Antibody potency relates to the ability to recognize the closed, prefusion form of HIV Env. *Nat Commun*. 2015;6:6144.
  64. Derking R, Ozorowski G, Sliepen K, Yasmeen A, Cupo A, Torres JL, Julien JP, Lee JH, van Montfort T, de Taeye SW, et al. Comprehensive antigenic map of a cleaved soluble HIV-1 envelope trimer. *PLoS Pathog*. 2015;11:e1004767.
  65. Lee JH, Ozorowski G, Ward AB. Cryo-EM structure of a native, fully glycosylated, cleaved HIV-1 envelope trimer. *Science*. 2016;351:1043–8.
  66. Andrewes CH, Elford WJ. Observations on anti-phage sera. II: Properties of incompletely neutralized phage. *Br J Exp Pathol*. 1933;XIV:376–83.
  67. Weiss JN. The Hill equation revisited: uses and misuses. *FASEB J*. 1997;11:835–41.
  68. Klein K, Veazey RS, Warrier R, Hraber P, Doyle-Meyers LA, Buffa V, Liao HX, Haynes BF, Shaw GM, Shattock RJ. Neutralizing IgG at the portal of infection mediates protection against vaginal simian/human immunodeficiency virus challenge. *J Virol*. 2013;87:11604–16.
  69. Klasse PJ. Modeling how many envelope glycoprotein trimers per virion participate in human immunodeficiency virus infectivity and its neutralization by antibody. *Virology*. 2007;369:245–62.
  70. Brandenberg OF, Magnus C, Rusert P, Gunthard HF, Regoes RR, Trkola A. Predicting HIV-1 transmission and antibody neutralization efficacy in vivo from stoichiometric parameters. *PLoS Pathog*. 2017;13:e1006313.
  71. Regoes RR, Magnus C. The role of chance in primate lentiviral infectivity: from protomer to host organism. *Prog Mol Biol Transl Sci*. 2015;129:327–51.
  72. Keele BF, Derdeyn CA. Genetic and antigenic features of the transmitted virus. *Curr Opin HIV AIDS*. 2009;4:352–7.
  73. Keele BF, Li H, Learn GH, Hraber P, Giorgi EE, Grayson T, Sun C, Chen Y, Yeh WW, Letvin NL, et al. Low-dose rectal inoculation of rhesus macaques by SIVsmE660 or SIVmac251 recapitulates human mucosal infection by HIV-1. *J Exp Med*. 2009;206:1117–34.
  74. Korber B, Gaschen B, Yusim K, Thakallapally R, Keshmir C, Detours V. Evolutionary and immunological implications of contemporary HIV-1 variation. *Br Med Bull*. 2001;58:19–42.
  75. Behrens AJ, Crispin M. Structural principles controlling HIV envelope glycosylation. *Curr Opin Struct Biol*. 2017;44:125–33.
  76. Behrens AJ, Struwe WB, Crispin M. Glycosylation profiling to evaluate glycoprotein immunogens against HIV-1. *Expert Rev Proteomics*. 2017;14:881–90.
  77. Seabright GE, Doores KJ, Burton DR, Crispin M. Protein and glycan mimicry in HIV vaccine design. *J Mol Biol*. 2019;431:2223–47.
  78. Ward AB, Wilson IA. Insights into the trimeric HIV-1 envelope glycoprotein structure. *Trends Biochem Sci*. 2015;40:101–7.
  79. Ward AB, Wilson IA. The HIV-1 envelope glycoprotein structure: nailing down a moving target. *Immunol Rev*. 2017;275:21–32.
  80. Kim AS, Leaman DP, Zwick MB. Antibody to gp41 MPER alters functional properties of HIV-1 Env without complete neutralization. *PLoS Pathog*. 2014;10:e1004271.
  81. Doores KJ, Burton DR. Variable loop glycan dependency of the broad and potent HIV-1-neutralizing antibodies PG9 and PG16. *J Virol*. 2010;84:10510–21.

82. Klasse PJ. The molecular basis of HIV entry. *Cell Microbiol.* 2012;14:1183–92.
83. Nguyen DN, Xu B, Stanfield RL, Bailey JK, Horiya S, Temme JS, Leon DR, LaBranche CC, Montefiori DC, Costello CE, et al. Oligomannose glycopeptide conjugates elicit antibodies targeting the glycan core rather than its extremities. *ACS Cent Sci.* 2019;5:237–49.
84. Poignard P, Moulard M, Golez E, Vivona V, Franti M, Venturini S, Wang M, Parren PW, Burton DR. Heterogeneity of envelope molecules expressed on primary human immunodeficiency virus type 1 particles as probed by the binding of neutralizing and nonneutralizing antibodies. *J Virol.* 2003;77:353–65.
85. Changeux JP, Edelstein S. Conformational selection or induced fit? 50 years of debate resolved. *F1000 Biol Rep.* 2011;3:19.
86. Frauenfelder H, Sligar SG, Wolynes PG. The energy landscapes and motions of proteins. *Science.* 1991;254:1598–603.
87. Hu X, Hong L, Smith MD, Neusius T, Cheng X, Smith JC. The dynamics of single protein molecules is non-equilibrium and self-similar over thirteen decades in time. *Nat Phys.* 2016;12:171–4.
88. Stock G, Hamm P. A non-equilibrium approach to allosteric communication. *Philos Trans R Soc Lond B Biol Sci.* 2018;373:20170187.
89. Metzler R. Forever aging. *Nat Phys.* 2016;12:113–4.
90. Do Kwon Y, Wang XE, Bender MF, Yang R, Li Y, McKee K, Rawi R, O'Dell S, Schneck NA, Shaddeau A, et al. Structures of HIV-1 neutralizing antibody 10E8 delineate the mechanistic basis of its multi-peak behavior on size-exclusion chromatography. *Antibodies.* 2021;10:23.
91. Fassolari M, Chemes LB, Gallo M, Smal C, Sanchez IE, de Prat-Gay G. Minute time scale prolyl isomerization governs antibody recognition of an intrinsically disordered immunodominant epitope. *J Biol Chem.* 2013;288:13110–23.
92. Guttman M, Padte NN, Huang Y, Yu J, Rocklin GJ, Weitzner BD, Scian M, Ho DD, Lee KK. The influence of proline isomerization on potency and stability of anti-HIV antibody 10E8. *Sci Rep.* 2020;10:14313.
93. Lu KP, Finn G, Lee TH, Nicholson LK. Prolyl cis-trans isomerization as a molecular timer. *Nat Chem Biol.* 2007;3:619–29.
94. Nicholson LK, Lu KP. Prolyl cis-trans Isomerization as a molecular timer in Crk signaling. *Mol Cell.* 2007;25:483–5.
95. Alegre-Cebollada J, Kosuri P, Rivas-Pardo JA, Fernandez JM. Direct observation of disulfide isomerization in a single protein. *Nat Chem.* 2011;3:882–7.
96. Go EP, Cupo A, Ringe R, Pugach P, Moore JP, Desaire H. Native conformation and canonical disulfide bond formation are interlinked properties of HIV-1 Env glycoproteins. *J Virol.* 2015;90:2884–94.
97. Go EP, Hua D, Desaire H. Glycosylation and disulfide bond analysis of transiently and stably expressed clade C HIV-1 gp140 trimers in 293T cells identifies disulfide heterogeneity present in both proteins and differences in O-linked glycosylation. *J Proteome Res.* 2014;13:4012–27.
98. Cimbro R, Gallant TR, Dolan MA, Guzzo C, Zhang P, Lin Y, Miao H, Van Ryk D, Arthos J, Gorshkova I, et al. Tyrosine sulfation in the second variable loop (V2) of HIV-1 gp120 stabilizes V2–V3 interaction and modulates neutralization sensitivity. *Proc Natl Acad Sci USA.* 2014;111:3152–7.
99. Allen JD, Sanders RW, Doores KJ, Crispin M. Harnessing post-translational modifications for next-generation HIV immunogens. *Biochem Soc Trans.* 2018;46:691–8.
100. Pritchard LK, Spencer DI, Royle L, Vasiljevic S, Krumm SA, Doores KJ, Crispin M. Glycan microheterogeneity at the PGT135 antibody recognition site on HIV-1 gp120 reveals a molecular mechanism for neutralization resistance. *J Virol.* 2015;89:6952–9.
101. Pritchard LK, Vasiljevic S, Ozorowski G, Seabright GE, Cupo A, Ringe R, Kim HJ, Sanders RW, Doores KJ, Burton DR, et al. Structural constraints determine the glycosylation of HIV-1 envelope trimers. *Cell Rep.* 2015;11:1604–13.
102. Cao L, Pauthner M, Andrabi R, Rantalainen K, Berndsen Z, Diedrich JK, Menis S, Sok D, Bastidas R, Park SR, et al. Differential processing of HIV envelope glycans on the virus and soluble recombinant trimer. *Nat Commun.* 2018;9:3693.
103. Behrens AJ, Vasiljevic S, Pritchard LK, Harvey DJ, Andev RS, Krumm SA, Struwe WB, Cupo A, Kumar A, Zitzmann N, et al. Composition and antigenic effects of individual glycan sites of a trimeric HIV-1 envelope glycoprotein. *Cell Rep.* 2016;14:2695–706.
104. Cao L, Diedrich JK, Kulp DW, Pauthner M, He L, Park SR, Sok D, Su CY, Delahunty CM, Menis S, et al. Global site-specific N-glycosylation analysis of HIV envelope glycoprotein. *Nat Commun.* 2017;8:14954.
105. van Gils MJ, van den Kerkhof TL, Ozorowski G, Cottrell CA, Sok D, Pauthner M, Pallesen J, de Val N, Yasmeen A, de Taeye SW, et al. An HIV-1 antibody from an elite neutralizer implicates the fusion peptide as a site of vulnerability. *Nat Microbiol.* 2016;2:16199.
106. Gaebler C, Nogueira L, Stoffel E, Oliveira TY, Breton G, Millard KG, Turroja M, Butler A, Ramos V, Seaman MS, et al. Prolonged viral suppression with anti-HIV-1 antibody therapy. *Nature.* 2022. <https://doi.org/10.1038/s41586-022-04597-1>.
107. Mendoza P, Gruell H, Nogueira L, Pai JA, Butler AL, Millard K, Lehmann C, Suarez I, Oliveira TY, Lorenzi JCC, et al. Combination therapy with anti-HIV-1 antibodies maintains viral suppression. *Nature.* 2018;561:479–84.
108. Zhou T, Georgiev I, Wu X, Yang ZY, Dai K, Finzi A, Kwon YD, Scheid JF, Shi W, Xu L, et al. Structural basis for broad and potent neutralization of HIV-1 by antibody VRC01. *Science.* 2010;329:81–7.
109. Huang J, Ofek G, Laub L, Louder MK, Doria-Rose NA, Longo NS, Imamichi H, Bailer RT, Chakrabarti B, Sharma SK, et al. Broad and potent neutralization of HIV-1 by a gp41-specific human antibody. *Nature.* 2012;491:406–12.
110. Pugach P, Marozsan AJ, Ketas TJ, Landes EL, Moore JP, Kuhmann SE. HIV-1 clones resistant to a small molecule CCR5 inhibitor use the inhibitor-bound form of CCR5 for entry. *Virology.* 2007;361:212–28.
111. Schmidt F, Weisblum Y, Muecksch F, Hoffmann HH, Michailidis E, Lorenzi JCC, Mendoza P, Rutkowska M, Bednarski E, Gaebler C, et al. Measuring SARS-CoV-2 neutralizing antibody activity using pseudotyped and chimeric viruses. *J Exp Med.* 2020;217:e2020118.
112. Sarzotti-Kelsoe M, Bailer RT, Turk E, Lin CL, Bilska M, Greene KM, Gao H, Todd CA, Ozaki DA, Seaman MS, et al. Optimization and validation of the TZM-bl assay for standardized assessments of neutralizing antibodies against HIV-1. *J Immunol Methods.* 2014;409:131–46.

## Publisher's Note

Springer Nature remains neutral with regard to jurisdictional claims in published maps and institutional affiliations.

Ready to submit your research? Choose BMC and benefit from:

- fast, convenient online submission
- thorough peer review by experienced researchers in your field
- rapid publication on acceptance
- support for research data, including large and complex data types
- gold Open Access which fosters wider collaboration and increased citations
- maximum visibility for your research: over 100M website views per year

At BMC, research is always in progress.

Learn more [biomedcentral.com/submissions](https://biomedcentral.com/submissions)

